

Bc. Alicia Rijo Estrella

Utilization of SAR Interferometry to identify and map landslides in Sánchez municipality, D.R.

VŠB – TECHNICAL UNIVERSITY OF OSTRAVA
FACULTY OF MINING AND GEOLOGY
INSTITUTE OF GEOINFORMATICS

Utilization of SAR Interferometry to identify and map landslides
in Sánchez municipality, Dominican Republic

Využití družicové SAR interferometrie pro identifikaci a
mapování sesuvů ve městě Sánchez, Dominikánské republice

Diploma Thesis
Ostrava, 2017

Autor:
Supervisor:

Bc. Alicia Rijo Estrella
Ing. Milan Lazecký, Ph.D

Study platform: Geodesy and cartography.
Study domain: Geoinformatic.

VŠB - Technical University of Ostrava
Faculty of Mining and Geology
Institute of Geoinformatics

Diploma Thesis Assignment

Student:

Alicia Rijo Estrella

Study Programme:

N3654 Geodesy, Cartography and Geoinformatics

Study Branch:

3608T002 Geoinformatics

Title:

Utilization of satellite SAR Interferometry to Identify and Map
Landslides in Sánchez Municipality, Dominican Republic
Využití družicové SAR interferometrie pro identifikaci a mapování
sesuvů ve městě Sánchez, Dominikánské republice

The thesis language:

English

Description:

The landscapes we see today are the result of constant changes during millions of years. Mass movement is one of the principal geomorphology process responsible for this changes and occurs in different scales around the world, causing disaster in populated areas.

Sánchez is a municipality located in Samaná province, Dominican Republic, where constant landslides had created an atmosphere of uncertainty among the inhabitants, that observed day after day the deterioration of infrastructures, loss of agricultural capability and potential life threatening situations. Slope instability has been increased by anthropogenic activity and triggers factors as: elimination of forest for coconut plantation, lack of proper waste drainage and drinking water supply system, growth of community, change of construction material, meteorological phenomena and seismic events.

This investigation aims to identify slope movement and map landslide activity, using Sentinel-1 satellite SAR interferometry (InSAR). By applying multi-temporal techniques to a series of Sentinel-1 images, it is possible to recognize a continuous surface deformation in the area. The results will help authorities to develop short and long term risk management plans.

The diploma thesis consists of following tasks:

- Achieve theoretical background of InSAR techniques, with the main focus on Persistent Scatterers (PS) and specifics of InSAR towards investigating landslide activity
- Perform PS processing of Sentinel-1 data over Sánchez municipality
- Evaluate achieved results: interpret estimated parameters and analyse correspondence of detected movements with ground truth information.
- Create map of potential slow landslide activity.

Extent of graphical output:
as needed

Extent of thesis:
50 - 70 standard pages

References:

KETELAAR, Virginia Bernard H. Satellite radar interferometry: subsidence monitoring techniques. New York: Springer, c2009. ISBN 978-1-4020-9427-9.

Bc. Alicia Rijo Estrella

Utilization of SAR Interferometry to identify and map landslides in Sánchez municipality, D.R.

WASOWSKI, J., BOVENGA, F. Investigating landslides and unstable slopes with satellite Multi Temporal Interferometry: Current issues and future perspectives. Engineering Geology, 174, 103-138, 2014, Elsevier. DOI: 10.1016/j.enggeo.2014.03.003.

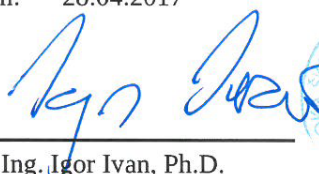
HIGHLAND, L.M., BOBROWSKY, Peter. The Landslide Handbook-A guide to understanding landslides. United States Geological Survey and Geological Survey of Canada. 2008

Extent and terms of a thesis are specified in directions for its elaboration that are opened to the public on the web sites of the faculty.

Supervisor: **Ing. Milan Lazecký, Ph.D.**

Date of issue: 31.10.2016

Date of submission: 28.04.2017



doc. Ing. Igor Ivan, Ph.D.
Head of Institute



prof. Ing. Jaroslav Dvořáček, CSc.
Acting Dean

Declaration of the author of this diploma thesis

- I have processed the whole diploma thesis myself, and I have mentioned all used documents and literature. I was acquainted with the fact that my diploma thesis is fully pursuant to Act No.121/2000 Coll. - Copyright Act, in particular Article 35 - Use of Work as Part of Civil and Religious Ceremonies or as Part of Official Events Organized by Public Authorities or during School Performances, and the Use of School Work and Article 60 - School Work.
- I am aware that Vysoká škola báňská - Technical University of Ostrava (hereinafter VŠB-TUO) has the right non-profitably, for its internal need, to use my diploma thesis (Article 35 paragraph 3).
- I agree that one copy will be kept by the supervisor of the diploma thesis. I agree that the details of the diploma thesis, contained in the Record on the Final Thesis, placed in the appendix of my diploma thesis, will be published in the information system of VSB-TUO.
- I agree that the diploma thesis is licensed under a Creative Commons Attribution-NonCommercial-ShareAlike 3.0 Unported License. To view a copy of this license it is possible to visit <http://creativecommons.org/licenses/by-nc-sa/3.0/>
- It was agreed that I will conclude a copyright license agreement with VSB-TUO, in the case of their interest to use my work commercially from their side, within Article 12 paragraph 4 of the Copyright Act.
- It was agreed that I can use my work - diploma thesis or provide a license to its commercial use only with the consent of VSB-TUO, who is entitled, in such case to require an appropriate contribution from me to cover costs, which were spent by VSB-TUO to create this thesis (up to their up-to-date level).

In Ostrava on

22/December/2017

Author's full name and signature



ABSTRACT

The landscapes we see today are the result of constant changes during millions of years. Mass movement is one of the principal geomorphology process responsible for these changes and occurs in different scales around the world, causing disaster in populated areas.

Sánchez is a municipality located in Samaná province, Dominican Republic, where continuous motion had created an atmosphere of uncertainty among the inhabitants, that observed day after day the deterioration of infrastructures, loss of agricultural capability and potential life-threatening situations. Slope instability has been increased by anthropogenic activity and triggers factors as: elimination of forest for coconut plantation, lack of proper waste drainage and drinking water supply system, growth of community, change of construction material, meteorological phenomena and seismic events.

This investigation aims to identify slope movement and map it, using SENTINEL-1 satellite SAR interferometry (InSAR). By applying multi-temporal techniques to a series of SENTINEL-1 scenes, it is possible to recognize a continuous surface deformation in the area. The results will help authorities to develop short and long-term risk management plans.

Key words: InSAR, landslides, Persistent Scatter, Sánchez municipality.

TABLE OF CONTENT

ABSTRACT	2
TABLE OF CONTENT	6
1 Introduction.....	1
1 Research problem.....	3
2 Research objectives.....	3
3 Justification for the present study	3
2 SAR Overview.....	4
2.1 Synthetic Aperture Radar	4
2.2 SAR Data.....	5
2.2.1 Satellite and mission	6
2.2.2 Acquisition modes and products	7
2.3 Microwave spectrum in SAR	8
2.4 Scattering.....	9
2.4.1 Atmospheric scattering	10
2.4.2 Scattering mechanisms.....	10
2.5 Geometry distortions	12
3 SAR Interferometry	13
4 Differential SAR Interferometry.....	15
4.1 Interferometric phase contributions.....	15
4.1.1 Geometry.....	16
4.1.2 Deformation	16
4.1.3 Atmospheric effect.....	17
4.1.4 Noise	18
4.2 InSAR limitations.....	20
4.2.1 Decorrelation.....	20
4.2.2 Orbital effect	22
4.2.3 Phase unwrapping errors	23
4.3 Persistent Scatter technique.....	24

4.3.1	PS advantages and limitations.....	24
5	Landslides overview	26
5.1	Application of InSAR for landslides	28
6	Sánchez municipality: case of study	30
6.1	Background settings	31
6.1.1	Geology and Tectonic	31
6.1.2	Geomorphology settings	34
6.1.3	Climatology and Hydrography.....	35
6.2	Sánchez landslides.....	37
6.2.1	Field observations	40
7	PSInSAR analysis.....	42
7.1	Available SAR data.....	42
7.2	Processing steps.....	43
7.3	PSInSAR results	47
8	conclusion and recommendations.....	51
8.1	Conclusion.....	51
8.2	Recommendations	52
	BIBLIOGRAPHY	53
	NOMENCLATURE.....	56
	List of symbols	56
	List of abbreviations.....	57
	LIST OF FIGURES	58
	LIST OF TABLES	59

1 INTRODUCTION

Sánchez municipality in Samaná province, Dominican Republic is affected by focal landslides along its territory causing distress in its inhabitants during or after every natural occurrence like heavy rains, tectonic movements or even in day to day life when they can see the structural stress of their homes.

Remote sensing method called InSAR with its technique PSInSAR, is possible to implement in order to detect displacement and velocity of the soil motion, using continuous reflecting objects. The deformation rate is probable to calculate in urban areas because infrastructures are temporally stable, so changes of millimeter are noticeable. However, there are limitations that affect the measurements, being temporal and spatial decorrelation the most outstanding.

This thesis seeks to explicate this technology, its application in Sánchez municipality and interpretation of the analysis to then map the results. The structure of the thesis is:

CHAPTER 1 Constitutes the introduction of the investigation, the problem it aims to solve, also the objectives and justification.

CHAPTER 2 In order to understand the mechanism of InSAR is important to know elementary concepts about the technology, the acquisition and type of data. It is also important to comprehend the way sensor perceived the elements in the Earth surface is influenced by inner and outer characteristics as: material of the scatter, wavelength type, atmosphere, sensor and Earth curvature.

CHAPTER 3 Explain the InSAR process in a conceptual and mathematical point of view, while explain key concepts that will be necessary for the analysis.

CHAPTER 4 This chapter explains the method DInSAR, which overcomes limitations of InSAR. It also explains the main limitations of interferometric approach, some able to estimate and remove and others that are managed by the researcher.

CHAPTER 5 Is an entrance to understand the outcome of InSAR analysis. Firstly, by refresh basic concepts of landslides phenomena as: description, stages, triggers and classification due to velocity and material. And secondly, the application of InSAR according to the type of motion and limitations.

CHAPTER 6 Seeks to present the Area of Interest (AOI) backgrounds as: location, geology, tectonic, geomorphology, weather and hydrography in order to correlated it with the InSAR results. In this chapter, is also present the field trip observations results in areas with “resent” motion.

CHAPTER 7 Present the analysis steeps taken during the investigation and set results and interpretation.

CHAPTER 8 Closing chapter, here conclusion and recommendation for future investigations are propose.

1 Research problem

Landslides or mass movement are geological and geomorphological complex events that occurs around Dominican Republic in different scales. Due to economical and human cost of this events, is necessary to identify and map susceptible areas, however limitations as economic resources, scale and technology has become a barrier in this study field. The significant development of remote sensing focus in landslides in the last 2 decades with ERS, ENVISAT, RADARSAT, ALOS, J-ERS, X-SAR, COSMO-SkyMed and SENTINEL-1 with free access data policy allowing research in developing countries. Research questions are formulated as:

- How can InSAR Persistent Scatter be used to identify landslides activities?
- It is possible to identify and map landslides in Sánchez municipality using InSAR?

2 Research objectives

The main objective of this investigation is to identify slope movement using Synthetic Aperture Radar Interferometry (InSAR). Specific objectives are:

- Achieve theoretical background of InSAR techniques, with the main focus on Persistent Scatters (PS) and specifics of InSAR towards investigating landslide activity.
- Perform PS processing of SENTINEL-1 data over Sánchez municipality.
- Evaluate achieved results: interpreted estimated parameters and analyze correspondence of detected movements with ground truth information.
- Created map of potential slow landslide activity.

3 Justification for the present study

- Incentive the use of new technology for landslides identification and monitoring in D.R.
- The result of this study will be of great value to Sánchez inhabitants and a contribution for future investigations.
- Created maps will be a good resource for governmental institutions dedicated to risk management.

2 SAR OVERVIEW

This chapter focus is an overview of Synthetic-aperture radar (SAR) in order to refresh or introduce briefly main concepts of this systems, without going into technical details beyond the scope of this investigation.

2.1 Synthetic Aperture Radar

Radio detection and ranging also known as RADAR, was first develop in the late 1940s with the purpose of using radio waves to detect objects position, course and distance (Lillesand et al, 2008). The process consists in emitting waves or pulse of microwave in a direction and record the echoes received within the system field of view. Subsequently, RADAR start to be used for remote sensing activities through advance data processing method called Synthetic Aperture Radar (SAR).

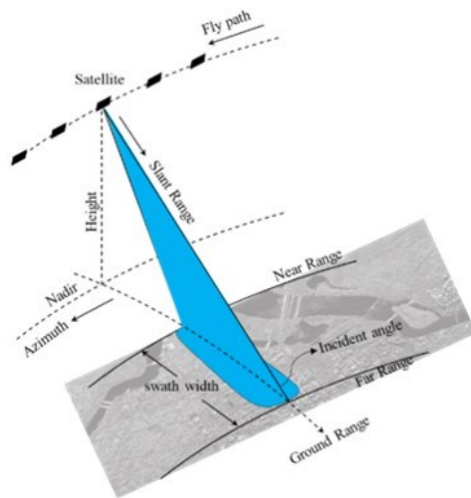


Figure 1. SAR geometry.

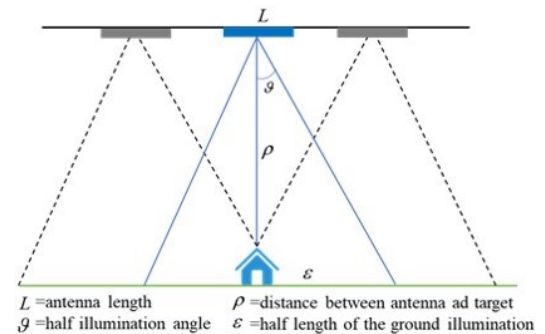


Figure 2. SAR synthetic antennas schema.

In Figure 1, it is possible to observe the main SAR geometry elements. The spaceborne/airborne instrument moves in a specific direction or path in direct line with its point on ground also known as Nadir. The microwaves beam is transmitted in a non-zero angle from Nadir, capturing a specific area or swath.

The distance in the direction of RADAR propagation is known as Range, this is perpendicular to the fly path and is composed by Near and Far Range according to its distance to the Nadir. Slant Range or Line of Sight (LOS), is the direct distance from the antenna to the object, while Ground Range measures the distance from the ground track of the platform to the object. The angle between the RADAR beam and ground surface is called Incidence angle.

SAR systems operate on the principle of using the sensor motion along track to transform a single physically short antenna into an array of such antennas that can be linked together mathematically as part of the data recording and processing procedures (Elachi, 1987 as cited in Lillesand et al, 2008), see Figure 2. The introduction of synthetic antennas in SAR enable the spacecraft with a small antenna to cover bigger areas with better spatial resolution, however, the movement of the spaceborne cause doppler shift, a change in wave frequency as a function of the relative velocities of a transmitter and a reflector (Lillesand et al, 2008), to solve this error the frequency of the pulse must be greater than the Doppler shift.

2.2 SAR Data

SAR scenes collect by the satellite are composed by a mosaic of small elements call pixels, each pixel denotes a small surface of the earth that is representing and contains amplitude and phase information.

- The amplitude is the strength of the return signal, influenced by the physical properties of the surface. The variability of the amplitude creates speckles, small granular aspect with random variations result of fluctuations in the return signal due to interference.
- Phase is the round-trip distance from the satellite to the ground and back of pulse measured in units of the radar wavelength. Scatters at different slant ranges introduce different time delays between transmission and reception of the radiation, this difference is called phase difference.

2.2.1 Satellite and mission

SAR data can be obtained through several Earth observation satellites previously mention, being SENTINEL-1 the instrument used to acquire SAR data for this investigation. As the first joint mission of the European Commission (EC) and the European Space Agency (ESA) under the Copernicus initiative, SENTINEL-1 is constitute by 2 spacecrafts: SENTINEL-1A and SENTINEL-1B, the first launch in 2014 while the second was launch 18 months later (ESA,2013).

Both spacecraft are a three-axis satellites compose by a sun, star, gyro and magnetic field sensors. The orbit and altitude control are keep with a set of four reaction wheels and three torque rods. Energy acquisition, is done through two solar array wings. In the Figure 3, a model of the spacecraft is present.

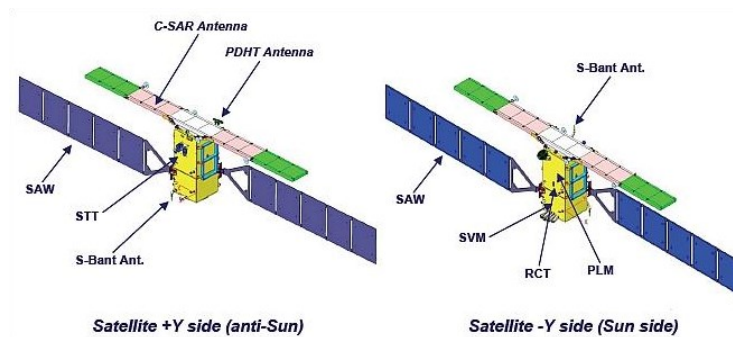


Figure 3. SENTINEL satellite

Source: report “Reprinted from ESA information”, 2017.

Reference orbit is maintained within an earth-fixed orbital tube of a diameter of 100 m (RMS) during normal operation(ESA,2013). Accurate pointing knowledge is greater than 0.004° on each axis, high pointing accuracy about 0.01° on each axis and real-time orbit determination together with a dedicated propulsion system for precise orbit control. SENTINEL-1 carries a C-band SAR sensor with a center frequency of 5.405 GHz, single and dual polarization in an angle between $20^\circ - 45^\circ$ and radiometric accuracy is 1dB. Their trajectory is Ascending and Descending.

2.2.2 Acquisition modes and products

SENTINEL-1 acquire data in 4 modes in 3 different processing levels:

- Level 0 is form by raw data with noise and information as: orbit information, internal calibration, echo source packets and altitude.
- Level 1, is the transformation through algorithms of level 0 data, includes pre-processing, Doppler centroid estimation, range and azimuth processing and post-processing.
- Level 2, is a derivation of level 1 products, its main use is for ocean data.

The modes are:

- Stripmap (SM): this mode consists in illuminated the swath ground with a continuous sequence of pulses while the antenna beam is pointing to a fixed azimuth and elevation angle (ESA,2013). Each swath has an area of 80km and a spatial resolution of 5x5m. Polarization options are single and dual.
- Interferometric Wide Swath (IW): acquired data in three swaths using the Terrain Observation with Progressive Scanning SAR (TOPSAR) imaging technique, this consist in bursts by cyclically switching the antenna beam between multiple adjacent sub-swaths (ESA,2013). The bursts are synchronized to ensure alignment of interferometric pairs. Each swath has an area of 250km and a spatial resolution of 5x20m. Polarization options are single and dual. Compare to SM, IW have lower resolution, however the amount of land coverage is higher.
- Extra Wide swath (EW): like IW, EW use TOPSAR imaging technique, however, the area of disquisition is over 400km, this affects the resolution to 20x40m. The focus of this mode is over polar zones and maritime areas with ice and oil splits.
- Wave (WV): acquired data in small Stripmap scenes called 'vignettes', due to the lack of points of reference in the sea to overlap scenes, the acquisition is made alternating incidence angles between near and far range (23° and 35°). Each vignette has an area of 20x20 km and a spatial resolution of 5x5m every 100 km along track. For Wind Fields and Surface Radial Velocity, the spatial resolution is 1x1 km. WV is the main mode to acquired ocean data.

SAR Level 1 scenes can in 2 forms, Single Look Complex (SLC) and Ground Range Detected (GRD), both available for modes SM, IW and EW. For WV, the only available data is in Level 2.

SLC data consist in SAR data focused into zero-Doppler direction and distributed in original slant-range coordinates geometry (that can be geo-referenced using orbit information), it includes amplitude and phase. GRD is projected based on the earth ellipsoid model and is distributed without phase, it presents a reduction in speckle noise and geometric resolution.

2.3 Microwave spectrum in SAR

SAR spaceborne/airborne are considered active sensors, meaning that the illumination source is emit by itself making possible the collection of data during day or night. The interaction of objects on the surface differs from one wavelength to another, millimeter wavelength radiation is easy scatter by vegetation due to the low penetration, while meter wavelength radiation penetrates with no problem (Comer and Harrower, 2013). The different bands use in SAR are listed and partially described in Table 1.

Active missions and bands during the time this investigation took course are: SENTINEL-1, RADARSAR-1 and RADARSAR-2 with C band; TerraSAR-X, TanDEM-X and COSMO-Skymed with X band; and ALOS-2 with L band.

Table 1. Common SAR frequency bands and uses.

Band	Frequency	Wavelength	Common uses
P	<400 MHz	1 m+	Penetration, soil moisture, biomass.
L	1-2 GHz	15-30 cm	Vegetation, deformation.
S	2-4 GHz	7.5-15 cm	
C	4-8 GHz	3.75-7.5 cm	Agriculture, deformation, topography.
X	8-12 GHz	2.5-3.75 cm	High resolution, topography
Ku	12-18 GHz	1.67-2.5 cm	Ocean and open water
Ka	24-40 GHz	0.75-1.11 cm	Snow/ice (airborne)
Mm	40-300 GHz	7.5-1 mm	

Source: Skolnik, 1990.

The orientation of the electric and magnetic field vectors defines the polarization of the propagation wave (Richards, 2009). According to direction of the vector, the surface material reflected waves change. In the Figure 4, is possible to observed the definitions of the polarization in respect of the surface and plane of incidence.

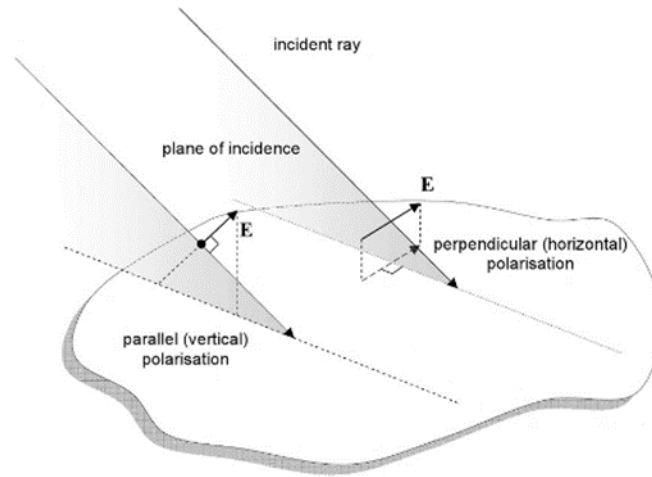


Figure 4. Polarization with respect of the incident angle and surface (Richards, 2009).

The electromagnetic radiation emits and receive by the RADAR system can be horizontal, vertical or both. Single polarization emits and receive the same polarization waves HH and VV, on the other hand, cross-polarization refers to combination of waves HV and VH. Typically, single polarization products are used for InSAR monitoring of displacements.

2.4 Scattering

The electromagnetic radiation can be reflected or diffuse during its travel from the sensor to the earth's surface and back. The received signal is a combination of many independent reflections in different stages of the travel. In this section Atmospheric scattering and scattering mechanisms will be covered.

2.4.1 Atmospheric scattering

In the atmosphere particles and gases can affect the wave emit by the sensor. Atmospheric scattering is the unpredictable diffusion of radiation by particles in the atmosphere (Lillesand et al, 2008). There are 3 types of atmospheric scatters:

- Rayleigh: cause by very small particles in the upper atmosphere, like dust nitrogen and oxygen.
- Mie scattering: occurs when particles (pollen, dust, smoke, water vapor) of the same size as the wavelength of the radiation intervene, occurs mostly in the lower part of the atmosphere.
- Nonselective scattering: happens with much larger particles as water drops and dust particles, creating fog in the image.

On the other hand, absorption mechanisms produce the opposite effect since the radiation is absorbs at a given wavelength, water vapor, ozone and carbon dioxide are the most efficient absorbers.

Once the electromagnetic energy overcomes the atmospheric mechanisms, 2 fundamental interaction with the earth surface takes place: reflection or scatter, absorption and/or transition. These interactions received the name of scattering mechanisms.

2.4.2 Scattering mechanisms

Remote sensing depends upon measuring the reflection or scattering of incident energy from earth surface (Richards, 2009), the energy scatter can be completely reflected or absorbed depending of the surface materials and the RADAR configuration (polarization and frequency). The common scattering mechanisms are:

- Specular reflection: depend on the surface roughness and its dielectric constant. For most rough surface the radiation is scatter away from the direction of the RADAR and only some reflected energy returns to the sensor.

- Volume scattering also referred as Diffuse scatter: occurs if the radar pulse penetrates into a 3-dimensional body. The energy is scattered multiple times in multiple directions, before parts of it are returned to the sensor. This is the typical situation of forest areas, where the leaves bounce the radiation in different directions.
- Double Bounce: is produce in smooth flat surface due to the fact that the RADAR pulse is reflect off of two perpendicular surfaces, reflecting most of the energy to the sensor.

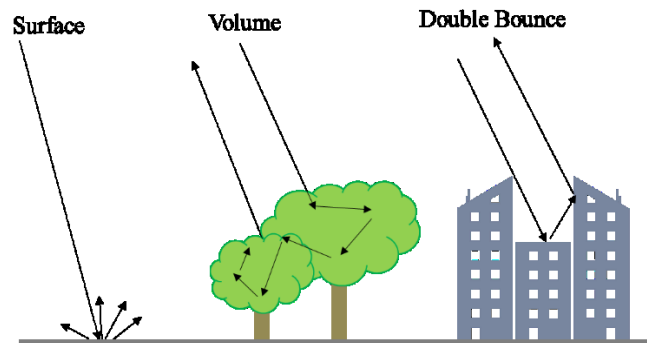


Figure 5. Common scattering mechanisms (based in Richards,2009).

Backscatter intensity is influenced by sensor parameters (specification of the RADAR system) and ground parameters (composition of the surface), See Table 2. Backscatter in urban areas is high, in forests is diffuse and dramatically reduce in water surfaces, roads, parking lots, etc.

Table 2. Backscattering parameters.

Sensor parameters	Ground parameters
Wavelength	Topography
Polarization	Surface roughness
Spatial resolution	Object geometry
Incident angle	Object orientation
Orbit	Dielectric properties

Source: ESA.

2.5 Geometry distortions

Like in any other remote sensing scenes, SAR scenes contains errors and/or distortions that makes them inaccurate. Geometric distortion may cause changes of scale over the image, irregularities in the angular relationships among the image elements, displacement of objects in an image and occlusion of one image element by another (A. L. Choo et al., 2012). The source of distortion can be cause by:

- The platform position and altitude.
- Sensor mechanisms and view geometry, also known as slant range distortion, is cause because measurements are taken side looking rather than horizontally, having as result a change in scale from Near to Far Range.
- Earth curvature, rotation and topographic effect (relief displacement), classified in:
 - Foreshortening: happens when the RADAR beam reaches the base before the top, resulting in compressed image and reduction in height of the observant object.
 - Layover: opposite to foreshortening, this occurs when the RADAR beam reaches the top before the base, resulting in displacement towards the RADAR from its real ground position.
 - RADAR shadow: cause by objects, these areas are not illuminate by the wavelength therefore no backscatter is received and no data collected.

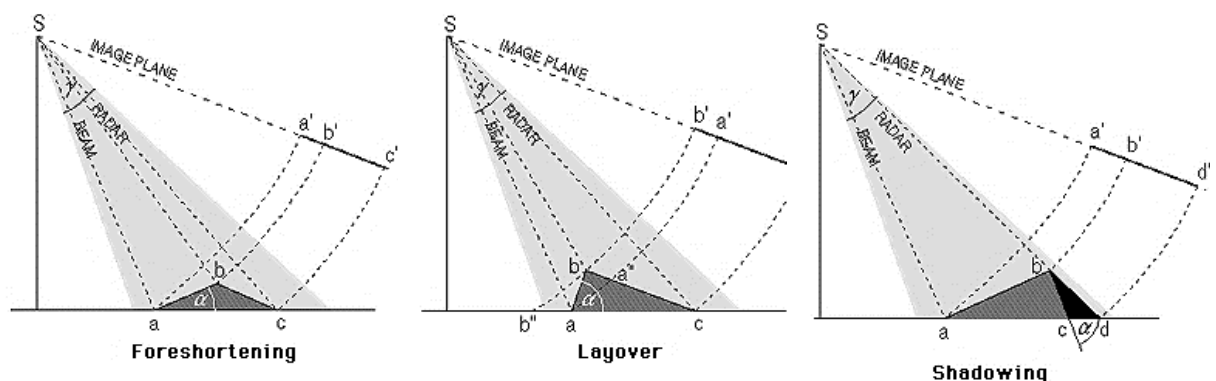


Figure 6. Topographic distortions.

Source: ESA handbook (<https://earth.esa.int/handbooks/asar/CNTR1-1-2.html>)

3 SAR INTERFEROMETRY

InSAR is based on the coherence of the RADAR signal, the recording of two scenes of the same area from different perspectives and the utilization of the phase information of the SAR scenes (Heim, 2010). This can be done simultaneously with 2 RADAR antennas, one acts as the receiver and the other as transmitter, or with only one RADAR antenna by repeating the orbits and acting as receiver and transmitter.

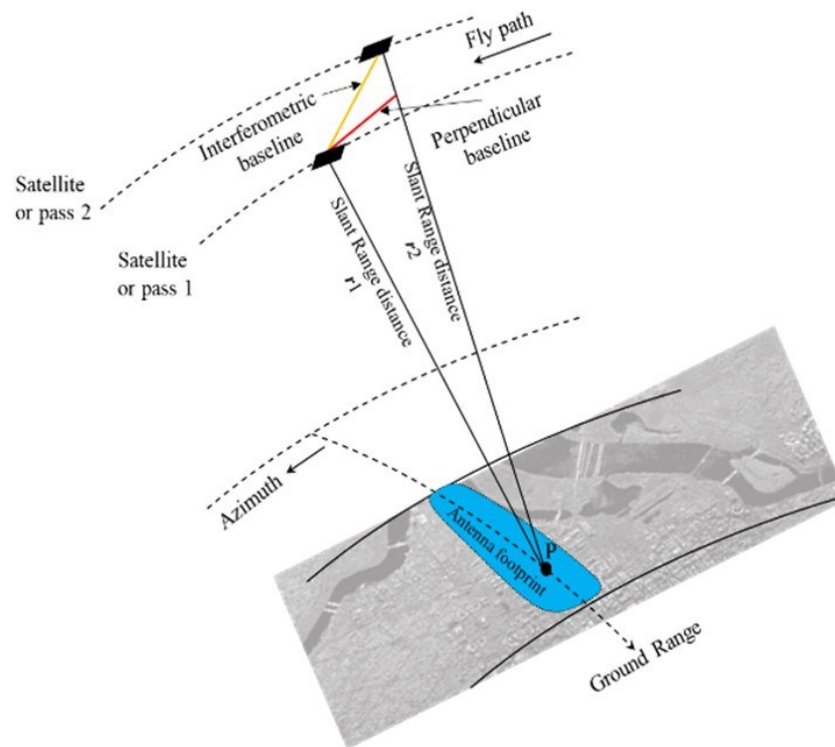


Figure 7. InSAR geometry.

Temporal separation of the two acquisitions receive the name Temporal baseline, the distance between the 2 satellites or pass called Interferometric baseline and its projection perpendicular to the slant range is called perpendicular baseline.

The electromagnetic pulse send to the earth has an integer number of complete wavelengths, once it interacts with the surface returns to the sensor has incomplete wavelength called phase.

The two-way travel of the wavelengths is equal to Equation 1, where (λ) is the transmitted wavelength and (r) is the range.

$$\phi = \frac{4\pi}{\lambda} r \quad \text{Equation 1}$$

The difference in round-trip range distance (r_1 and r_2) between 2 radar antennas and the earth surface multiply by the phase cycle is equal to the phase difference.

$$\phi_1 - \phi_2 = \Delta\phi = \frac{4\pi(r_1 - r_2)}{\lambda} = \frac{4\pi\Delta r}{\lambda} \quad \text{Equation 2}$$

The angular differences between the point (P') at a reference body and a point (P) at a height above the reference body, with the same range to the sensor provide information about topography. SAR instruments, however, are not capable to measure small angular differences, so information needs to be derivate form the distance measure between sensors and the resolution cell on Earth. In order to compare the pair of scenes, the sampling grid must be as congruent as possible, so Coregistration and resampling is necessary.

$$z_1 = z_M z_S^* = A_M A_S e^{i(\psi_M - \psi_S)} = A_I e^{i\phi} \quad \text{Equation 3}$$

The complex interferogram (z_1) compute by multiplying the master scene amplitude (M) by the complex conjugate of the slave (S)scene.

4 DIFFERENTIAL SAR INTERFEROMETRY

DInSAR is the method to extract displacement signature from a SAR interferogram over the acquisition period. Its origin was the product of a lack in Digital Elevation Model (DEM) with good resolution, so the reference phase could only be obtained through the ellipsoid and the surface displacement through derivation of complementary differential interferograms.

Differential interferograms can be construct with 3 methods:

- Two-pass method: use an external elevation model that is converted into radar coordinates, scaled using the baseline, and subtracted from the interferogram (Massonnet et al., 1993 as cite in Hanssen, 2001). The use of DEM however, may introduce error that can be interpreted as ground deformation.
- Three-pass method: use 3 SAR scenes, where two of them with no deformation, proper baseline and good coherence are used to create a *topographic pair*. This pair is unwrapped, scaled to the baseline characteristics of the *deformation pair*, and subtracted from it, yielding the differential interferogram, the so-called differential pair (Hanssen, 2001). The Three-pass method can only be use when the topographic and deformation pair has a common reference scene and it must be considered the influence of scaling.
- Four-pass method: is used when the topographic and deformation pair has no common reference scene, due to a large baseline of the pairs.

4.1 Interferometric phase contributions

The interferometric phase observations present a number of effects due to sensor, processing and surrounds. In this section I will concentrate in different contributions introduced by the surrounds, which is composed by: geometry, deformation, atmosphere and noise.

$$\Delta\phi = \Delta\phi_{geom} + \Delta\phi_{defo} + \Delta\phi_{atmo} + \Delta\phi_{noise} \quad \text{Equation 4}$$

The most important contribution is the geometry between the resolution element in the earth and the antenna. Secondly, the acceleration or delay of the signal due to the atmosphere. Thirdly, the change in scatter due to modification of the surface and lastly the superposition of scatters in the resolution cell.

4.1.1 Geometry

Characterized by the interferometric baseline and determined by the spatial location of the master scene, slave scene and point P, is the biggest contribution to the interferometric phase.

The contribution of the geometry is calculated by removing the reference phase cause by the earth curvature with precise orbits or a DEM, however residual errors as topography ($\delta\phi_{topo}$) and orbit ($\delta\phi_{orb}$) remains.

$$\varphi := \phi - \phi_{ref} = \delta\phi_{topo} + \delta\phi_{orb} + \phi_{defo} + \phi_{atmo} + \phi_{noise} \quad \text{Equation 5}$$

$\delta\phi_{topo}$ can be estimated and eliminated in time series approaches, because the DEM used is equal for every scene, in the case of $\delta\phi_{orb}$, however, the behavior is random for every acquisition.

In order to identify the terrain surface, the geometry phase is divided in: flat earth phase, contribution of the reference ellipsoid and topographic phase, and contribution of the topography above the ellipsoid.

4.1.2 Deformation

The relative displacement of scatters in the direction of the LOS inside the interferogram can be interpreted as ground deformation. When point P have a displacement between observations, there is an additional contribution to the interferometric phase variation.

$$\phi_{defo} = -\frac{4\pi\Delta r}{\lambda} D \quad \text{Equation 6}$$

Where (D) is the displacement vector project on the slant-range direction. Rapid and slow movements as earthquakes, landslides, subsidence, etc. have an extend between hundreds of meters to kilometers.

4.1.3 Atmospheric effect

When two interferometric SAR scenes are not simultaneous, the radiation travel path for each can be affected differently by the atmosphere. In particular, different atmospheric humidity, temperature and pressure between the two takes will have a visible consequence on the interferometric phase (Ferreti et al, 2007). Temperature and pressure are generally easy to dispense in comparison with humidity.

Even though the wavelength interacts with all the layers in the atmosphere, the contribution is basically induced by the Troposphere and the Ionosphere, introducing noise that affects the measures of altitude and surface deformation. The contribution of the Troposphere is the delay of the signal, while the Ionosphere is the acceleration of it.

Is well known that the Troposphere is the lowest layer of the atmosphere, where most of the weather condition happens and almost all clouds (cumulus and convective) are contained, for this reason it is charged with humidity, making it the main source of known atmospheric contribution. Convective clouds water content is low, causing almost no error in SAR signal, however, cumulus clouds can range from 0.5 to 2.0 gm/m³ causing delay of up to 11 mm/km in C band.

Table 3. Phase delay according to atmospheric conditions.

Delay source	Max delay (mm/km)	Delay source	Max delay (mm/km)
Dry air	290	Haze	0.02
High water vapor	140	Drizzle	0.2
Low water vapor	15	Steady rain (<20 mm/h)	2
Cloud	8	Heavy rain (<200 mm/h)	11 (C-band)
Advection fog	0.3	Hail	~5 (C-band)
Volcanic ash	0.101	Snow	~1 (C-band)

Delay source	Max delay (mm/km)	Delay source	Max delay (mm/km)
Sand	18	Aerosols	0.1

Source: Lazecký, 2011.

The acceleration caused by the Ionosphere produce a range error proportional to the total electron content (TEC) in the ionosphere (Ding et al. 2008). Ionospheric effects are large scaled, they cause phase distortions in distances larger than 100 km, sometimes also around 1 km streaks can be observed in azimuth direction (Gray et al., 2000 cited in Lazecký, 2011).

Ding et al. 2008, in the paper “Atmospheric Effects on InSAR Measurements and Their Mitigation” list various methods to mitigated the atmospheric effects based on: external data (ground meteorological observations), GPS data, results from numerical meteorological modeling, satellite water vapor products such as MERIS and MODIS and methods based in simple data analysis (pair-wise logic, stacking correlation and PSInSAR). The method to used depends on the atmospheric conditions, the number of scenes, external data available and the InSAR method used.

4.1.4 Noise

Phase noise are related to different types and existence of scatters in the scene, the main noise sources are due to:

- Temporal change of scatters: also known as temporal decorrelation, this noise is produce because the scatters change continuously in a short period of time, as in dense vegetated areas and water basins.
- Different look angle: the critical baseline for the scenes acquisition must be taken in consideration according to the sensor, if not the interferometric phase will be only noise.
- Volume scattering: explain in section 2.4.2.
- Nature of interaction with the ground: change in the refractive index of the scatters, due to different dielectric properties or distance from the satellite.

Methods to reduce noise phase are applied in different stages of the processing, these are:

- Range filtering: it basically removes parts of the image spectra that does not possess a counterpart between scenes, this is done because interferometry can only be perform with the same continuous scatters.
- Azimuth filtering: convergent orbit trajectories and different antenna squint angles (Doppler centroids), are the 2 effects result of variation in view direction. During the focusing, the scenes has already been filtered in azimuth to eliminate ambiguities and reduce noise, and passband has been center at individual Doppler centroid frequencies (Bamler et al, 1993 as cited by Bähr, 2013). Doppler centroids cause decorrelation because of the narrowed overlapping of the data spectra, add an extra orbit convergence can amplify or compensate the effect by adding a relative shift. Doppler centroids however, is not a problem for modern sensor, so it can't be considered for SENTINEL-1. Range and azimuth filtering increase the coherence if the resolution cell is dominate by surface scatters, in the case of point scatters, is not necessary because the coherence does not depend of the view RADAR direction.
- Multilooking: this method enhances the radiometric accuracy of SLC data, but reduce geometric resolution and spatial averaging. The equation for multilooked interferogram is:

$$\bar{z}_I(\bar{\varepsilon}, \bar{n}) = \frac{1}{m_\varepsilon m_n} \sum_{(\varepsilon, n) \in W} z_I(\varepsilon, n) \quad \text{Equation 7}$$

Where $m_\varepsilon m_n$ are the azimuth and range, and $W = \{(\varepsilon, n): (\bar{\varepsilon} - 1) m_\varepsilon < \varepsilon \leq \bar{\varepsilon} m_\varepsilon \wedge (\bar{n} - 1) m_n < n \leq \bar{n} m_n\}$. The Multilooking can be applied to complex interferograms, saving time in computation but reducing accuracy. Is important to take in consideration that if significant variations in small signals as atmosphere or deformation are average with this method, reduce the coherence, so the pixel size cannot exceed the spatial wavelength of the interest signal.

- Phase filtering: interferometric fringes patterns can be enhanced for phase unwrapping using reference phase and after applying a filter. The purpose of the filter is amplifying the dominant fringe frequency, reducing decorrelation noise.

4.2 InSAR limitations

Once the phase contributors have been corrected, other effects that contribute to error in the processing are: decorrelation, orbital effects and phase unwrapping errors, however, these are least controllable and are mostly in hands of the researcher how to approach them.

4.2.1 Decorrelation

Correlation is the relationship between the scattered electromagnetic fields seen at the interferometric receivers after image formation (Simons et al., 2007), in other words, when an area on the ground appears to have the same surface characterization in all scenes under analysis. The coherence can be used as a measure for the accuracy of the interferometric phase or as a tool for image classification (Hanssen, 2001).

Aside from the previous mentioned contributions, ϕ_{geom} , ϕ_{deform} and ϕ_{atmo} , the interferometric phase also contains other contributions, nevertheless, these can be modelled or doesn't have any spatial correlation property, causing them to be assume as ϕ_{noise} . In order to measure the correlation often referred as coherence ($|\gamma|$), between the masters and slave scene, Equation 8 is used.

$$\gamma = \frac{E\{z_M z_S^*\}}{\sqrt{E\{z_M z_M^*\} E\{z_S z_S^*\}}}, \quad \langle 0 \leq |\gamma| \leq 1 \rangle \quad \text{Equation 8}$$

Assuming both ergodicity and local spatial stationarity, the actually unknown expectation values $E\{\cdot\}$ can be approximated for a resolution cell with pixel coordinates (ε, n) by averaging over a spatial estimation window (Hanssen, 2001 as cited by Bähr 2013) of odd dimensions (m_ε, m_n) .

$$|\hat{\gamma}|(\epsilon, n) = \frac{\sum(i, j) \epsilon w^{Z_{M,ij} Z_{S,ij}^*}}{\sqrt{(\sum(i, j) \epsilon w^{Z_{M,ij} Z_{M,ij}^*})(\sum(i, j) \epsilon w^{Z_{S,ij} Z_{S,ij}^*})}} \quad \text{Equation 9}$$

where $W = \{(i, j) : |\epsilon - i| \leq (m_\epsilon - 1)/2 \wedge |n - j| \leq (m_n - 1)/2\}$.

The effects contributions to the ϕ_{noise} are calculate with the formula proposed by (Simons et al, 2007):

$$\gamma = \gamma_N \gamma_G \gamma_Z \gamma_T \quad \text{Equation 10}$$

Where:

γ_N =Correlation influenced by noise in the radar system and processing approach.

γ_G =Different observing geometries / terrain properties.

γ_Z =Influence of vertical extent of scatters (volume).

γ_T =The time between image acquisitions.

Decorrelation cause by noise in the Radar system and processing approach (γ_N .) Noise in the RADAR system is a combination of thermal noise, induce by the system gain factors and antenna characteristics and Doppler and range ambiguities. In case of processing approach, errors are due to algorithm selection for Coregistration, interpolation, image pre-processing and so on.

(γ_G) is the result of modification of the terrain reflectivity, due to the short wavelength of the radar signal, even slight changes of the looking angle may determine very different reflections (Perissin et al. 2006, 2014). The geometric correlation term is present for all scattering situations, and depends on the system parameters and the observation geometry (Simons et al, 2007).

The volumetric correlation (γ_Z) term can be understood in terms of an effective increase in the size of the projected range cell because the scattering elements in a given range cell are now extended not just on a surface but in a volume (Rosen et al., 2000 cited by Simons et al, 2007).

Typical case of volumetric decorrelation are vegetated areas, where the scatter of the canopy change constantly.

Temporal decorrelation (γ_T) occur due to modifications of the terrain properties between scenes acquisitions, causes can be either natural or artificial as fast ground movements, infrastructure constructions, agricultural field before and after tilling, etc.

The magnitude of the correlation(γ) in a group of pixels of a stable target is 1, while unstable target is $\gamma=0$. For convenience each decorrelation source is define as $\delta_x=1-\gamma_x$, where x can be N, G, Z or T.

4.2.2 Orbital effect

Generally, interferograms also present a sensor effect that cause stripping in the image according to the orbits of the antenna. To eliminate this effect, an operation called interferometric flattening takes place, generating fringes in proportional elevation range.

Interferogram flattening or flat-earth removal can be categorized into 2 classes: first using the parameters of the orbit and dealing with the interferogram directly, and second, estimate the position of the maximum frequency in the interferogram spectrum where the flat earth phase will dominate and then remove the phase reference (Zhang, 2005). Either method presents its own advantages and disadvantages that are further from the scope of this investigation.

The altitude between 2 adjacent fringes after the interferometric flattening is called altitude ambiguity (Δh_a), it is inversely proportional to the perpendicular baseline (B_n) and generates a phase rotation equal to 2π , where (r) is range between Earth and the satellite, (λ) is the instrument wavelength, (θ) is incidence angle.

$$\Delta h_a = \lambda * r * \sin(\theta) / 2B_n \quad \text{Equation 11}$$

Accuracy of the altitude measurement depends on the interferometric baseline. In the case of SENTINEL-1, its orbital tube is relatively narrow, reaching maximal values around $B_n=100$ m.

This induces a maximum $\Delta h_a=110$ m which means a relatively small sensitivity to the topographic altitude.

After eliminated topography signal, the residual phase should contain only signal due to displacements, atmospheric disturbances and noise. This signal is measured within the wavelength limits. In order to identify signal exceeding the wavelength, it is necessary to compute number of fringe cycles and correct phase values using step called phase unwrapping by some of existing algorithms. The noise can be partially removed using some spatial filtering algorithm.

4.2.3 Phase unwrapping errors

In order to identify signal exceeding the wavelength and know how many times it looped around the circle before it was finally measure by the sensor it is necessary to compute number of fringe cycles and correct phase values. This is important because targets at different heights can appear at the same phase.

Generally, the phase unwrapping method is done by selecting a starting location with a bright and clear phase and little noise, then in expanding contour add the multiple of 2π minimizing the phase change between pixels. After the unwrapping, still a global ambiguity is residual, this can only be remove by ground control points.

The unwrapping errors arise when:

- The phase is very noisy making the selection of a starting point really difficult.
- Sudden jump in the phase cause the interpolation to be erroneous.
- Wrong unwrapping technique selection. The most common are: Iterative Disk Masking, Goldstein, Minimal cost flow, Nearest Neighbor, Residue-cut and Least Squares.

Unwrapping process can lead to loss of signal over areas with visible fringes, making it hard to interpreted. In areas with very slight relief or with little deformation using differential interferograms is not always necessary to unwrap.

4.3 Persistent Scatter technique

PSI is a multitemporal InSAR technique created to overcome decorrelation and atmospheric contribution introduced in the phase values. It works by searching the imagery and interferograms for pixels that display stable amplitude and coherent throughout every image of the data set, receiving the name of Persistent Scatters (PS).

PS algorithms operate on a time series of interferograms all formed with respect to a single “master” SAR image. It is ultimately the level of decorrelation noise that defines whether pixels are PS pixels or not, but an initial selection of candidate PS pixels can be made using various proxies, the most common of which is amplitude dispersion (Ferretti et al. 2001; Hooper et al. 2012).

The main outcomes of a PSI analysis include the deformation time series, the deformation velocity and Residual Topographic Error (RTE), (difference between the true height of the scattering phase center of a given PS and the height of the DEM in this point).

4.3.1 PS advantages and limitations

PS present some key advantages like: cost (PS is relatively cheap compared with other technologies), wide-area coverage, sensitivity to small deformations (up to 1mm/yr.) and data is periodically provided (Crosetto et al.,2009). The limitations faced by PS techniques are:

- SAR data availability: refers to the scenes characteristics, like time interval, orbit (PS can only be performed with scenes in the same orbit) and quantity of scenes being 15 the minimum.
- PS availability: PS is able to measure deformation only over the available PSs, that is the points where PSI phases are good enough to get reliable deformation estimates. PS density is relatively high in urban areas, while it is usually low in vegetated and forested areas, over low-reflectivity areas (very smooth surfaces), and steep terrain (Crosetto et al.,2009).

- Deformation rates: fast deformation phenomena can be interpreted as error during the unwrapping phase. For SENTINEL-1, the differential deformation rate is 42.3 cm/year. When deformation exceeds the limit is necessary to rely on the amplitude information.
- Line-of-sight deformation: deformation can only be perceived if is in the LOS of the SAR sensor.
- Deformation movement: cause by uncompensated orbital errors or uncompensated low frequency atmospheric effects. It can be overcome by using multiple overlapping tracks or by fusing the PSI with external data.
- Thermal expansion: displacements caused by temperature differences in the area between scenes.

5 LANDSLIDES OVERVIEW

A landslide is a downward and outward movement of slope-forming composed of natural rock, soil, artificial fills or combinations of these materials under the influence of gravity (Marui 1988 cited from Varnes, 1996). Soil in slope areas are subject to gravitational stress, its adhesion characteristics make possible the stability of the slope, however the inclusion of more stress from others sources produce a lost in adhesion and therefore a mass movement.

Causes of landslides can be intrinsic and direct (FAO,1988). Intrinsic causes are geology and topography. Geological weak zones with numerous faults and fractures are more likely to produce landslides due to sudden movements, also the slope consolidation materials play an important role, sediment and poorly cemented rocks are more prone to movement. In case of the topography, areas in step slopes have higher gravitational stress.

Direct causes are, however, the key element to disturb the stability of the slope, this can be: groundwater, that saturates the soil and increase the pore water pressure; water erosion: landslides cause by the erosion of the slope support; and artificial or anthropogenic causes: construction of infrastructure, change in slopes, change in vegetation, leaking pipes, etc.

The four different stages for a landslide occurrence are (Rotaru et al, 2007):

- Pre-failure: soil mass is still continuous and controlled by progressive failure and creep. In this stage the pressure is building in the affected area.
- Failure stage: the formation of a continuous shear surface through the entire soil or rock mass. The breakage takes place and the soil starts to move.
- Post-failure: includes movement of the soil or rock mass involved in the landslide, from just after failure until it stops.
- Reactivation: the soil or rock mass slides along one or several pre-existing shear surfaces. This reactivation can be occasional or continuous with seasonal variations of the rate of movement.

Several classification systems have been proposed to help identify slope movements and mitigate its effects, being Varnes classification the most suitable for this investigation. Based in slide velocity (see Table 4) and type of movement (see Table 5).

The velocity of the slide change during its occurrence, in the first stages the sliding mass is really fast and then starts to reduce until it reaches a stable position. The maximum velocity depends on the slope angle, the angle between the horizontal and the ground surface. Velocities are directly associate with strength loss, due to liquefaction of granular material or sensitive clay and cohesion loss. The fastest the landslide, the more destructive.

Table 4. Slope movements respect to the slide velocity.

Speed class	Description	Velocity	Velocity (mm/sec)
1	Extremely slow	< 0.06 m/year	5×10^{-7}
2	Very low	0.06 m/year to 1.5 m year	
3	Slow	1.5 m/year to 1.5 m/month	5×10^{-5}
4	Moderate	1.5 m/month to 1.5 m/day	5×10^{-3}
5	Rapid	1.5 m/day to 0.3 m/min	5×10^{-1}
6	Very rapid	0.3 m/min to 3m/sec	5×10^1
7	Extremely rapid	> 3 m/sec	5×10^3

Source: Varnes (1996).

The types of movement are dependent of slope gradient, type of material and hydrological conditions.

Table 5. Classification of slope movements.

Types of movement	Type of material		
	Bedrock	Engineering soils	
		Predominantly coarse	Predominantly fine
Fall	Rock fall	Debris fall	Earth fall
Topples	Rock topple	Debris topple	Earth topple
Slides			
-Rotational	Rock slump	Debris slump	Earth slump
-Translation	Rock block slide	Debris block slide	Earth block slide
	Rock slide	Debris slide	Earth slide

Types of movement	Type of material		
	Bedrock	Engineering soils	
		Predominantly coarse	Predominantly fine
Lateral spreads	Rock spread	Debris spread	Earth spread
Flows	Rock fall	Debris flow	Earth flow
	(deep crack)	(Soil creep)	(soil creep)
Complex	Combination of two or more principal types of movement		

Source: Varnes (1996).

5.1 Application of InSAR for landslides

Landslides can be considered a challenge for Interferometric SAR, due to the fact that the ground deformation can exceeds the phase gradient limit eliminating the correlation. Because of this, several techniques have been developed according to the type of mass movement.

For fast moving landslides where the velocity limits of phase are exceeded, the density of stable pixels decreased significantly, as result the phase unwrapping is unsuccessful and fast mass movements can be considered processing errors. For this cases amplitude-based SAR techniques as: speckle tracking, sub-pixel offset and hybrid-SAR technique are the best options.

In the case of slow moving landslides phase based techniques as: PSInSAR, SqueeSAR, Small Baseline Subset(SBAS), the Stanford method for Persistent Scatterers (StaMPS) and interferometric point target analysis (IPTA) are recommended (Qu et al.,2016).

The multi-image PSInSAR technique has shown its capability to provide information about ground deformations over wide areas with millimetric precision, making this approach suitable for both regional and slope scale mass movements investigations (Tofani, 2013). For this reason, it has been selected to analyze deformation caused by mass movements.

Important limitations in the use of InSAR for landslide monitoring are:

- InSAR sensor has 2 types of fly direction: ascending, when satellite is moving in north direction and the LOS is to the west; and descending, when the satellite is moving to the south and looking to the east. Unfortunately, the sensor can only measure one-dimension displacement in the LOS, but the surface change in 3 dimensions (east and west, north and south, up and down), therefore, is impossible to determine the direction of the movement with only 1 interferogram. To overcome this is necessary to use GPS measurement data or combine different data direction.
- Vertical and horizontal motion are possible to observe if the LOS is perpendicular to ground motion, for this reason some direction movements are not detectable. In the Figure 8, a graphical explanation, where the blue arrow represents the LOS motion measure by the RADAR and the red arrow represent the terrain motion.

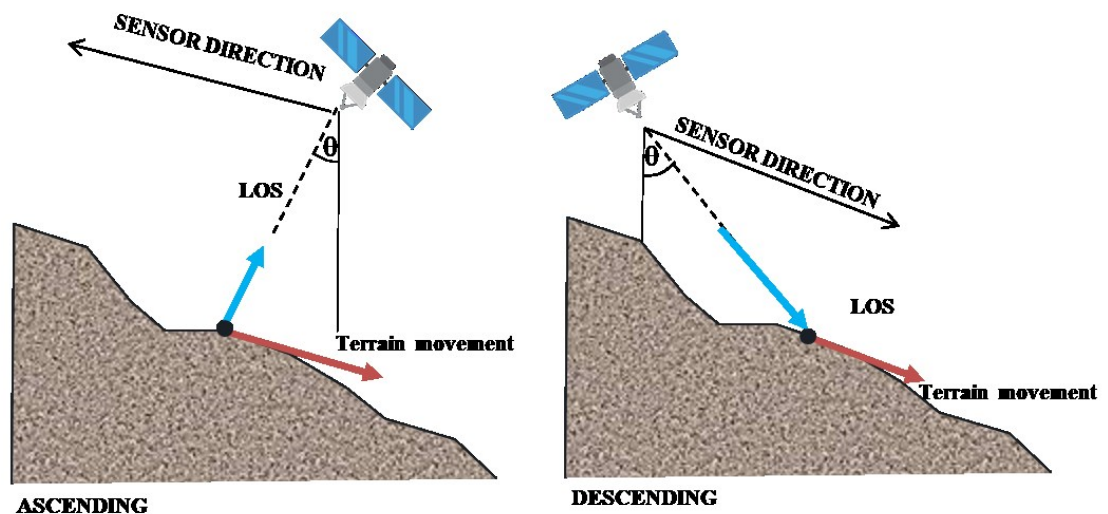


Figure 8. Measurement of motion.

- The motion can only be measure with certain temporal and spatial characteristics, relate to the sensor and the interval of the scenes. To calculate motion, is necessary that the time between acquisitions is not too big, the wider the time the higher the decorrelation.

6 SÁNCHEZ MUNICIPALITY: CASE OF STUDY

Locate in the northeast of Dominican Republic, Sánchez municipality was created in September 9th 1908 by law 4803c. It is one of the three municipalities that constitute Samaná province, aside from Las Terrenas and Samaná.

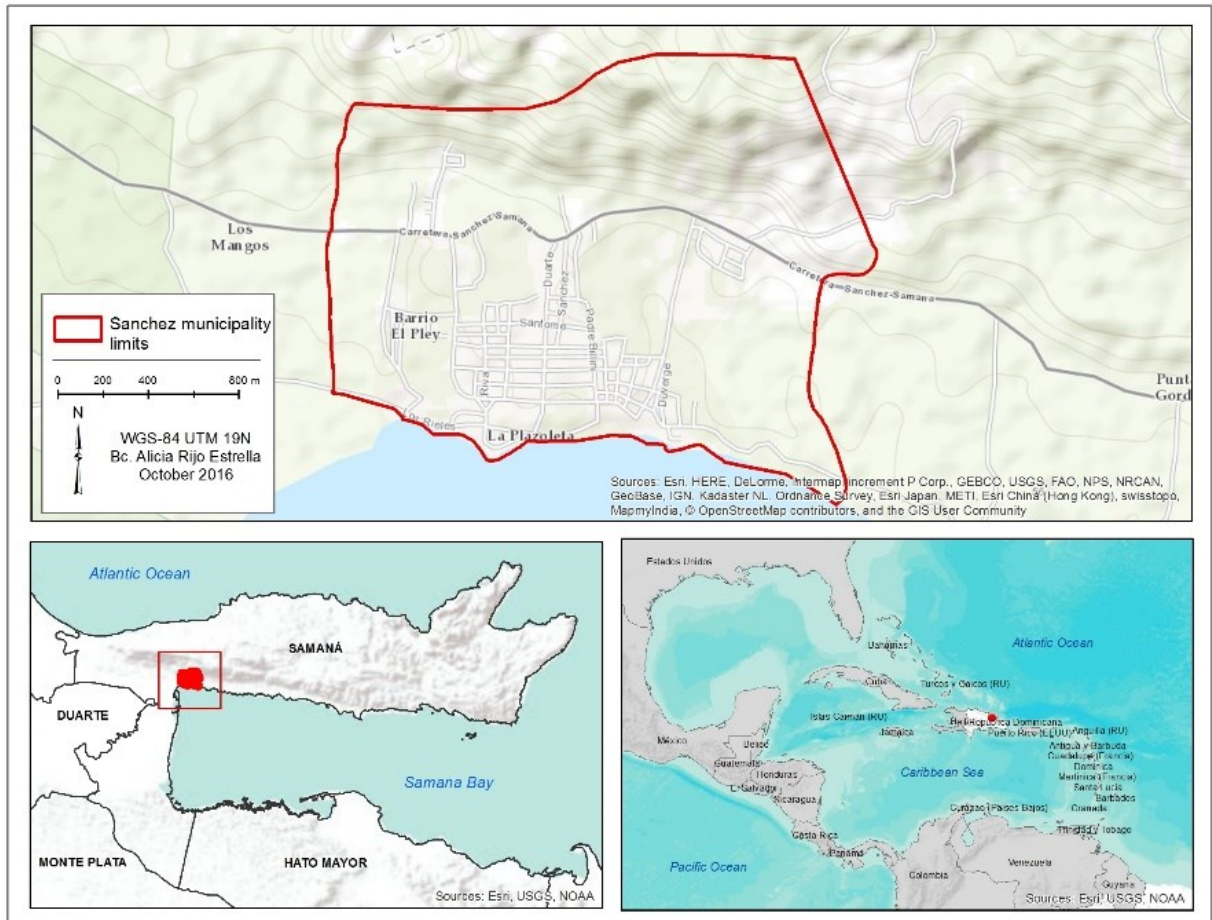


Figure 9. Localization map.

According to the IX National Census, in 2010, there were 24,509 inhabitants in the municipality, however, the majority is conglomerated in 2 main cities: La Majagua and Sánchez city, being the last one the head of the municipality and the Area of Interest (AOI) of this research with approximately 2km². The economy of AOI is based in: fishing, agriculture (mainly coconut) and tourism in small scale.

6.1 Background settings

Due to the contribution of natural triggers in landslides occurrence, is necessary to briefly explore the background settings where the AOI is locate, this introduction will also help to understand and explain possible outcomes of the InSAR analysis in the area.

6.1.1 Geology and Tectonic

Hispaniola island, occupied by two countries: Dominican Republic and Republic of Haiti, is located in the Caribbean Plate and subdivided in 2 microplates: Gonaives microplate and North Hispaniola microplate (Benford, 2012). Samaná Peninsula is completely contained in North Hispaniola microplate which is limited by 2 major faults: to the south the Northern Samaná Bay fault, a strike-slip faults; and to the north, the North Hispaniola fault, a subduction area of the Atlantic lithosphere beneath Hispaniola.

The tectonic of the peninsula is associate with an east-west-trending fault called Northern Samaná Bay fault and numerous small northeast-southwest and northwest-southwest trending faults that cuts both metamorphic and late Tertiary sediments (Joyce,1991 cited from Llinas,1983). The tectonic of the area is active generating uplift and in consequence numerous small earthquakes every year (SGN, 2010).

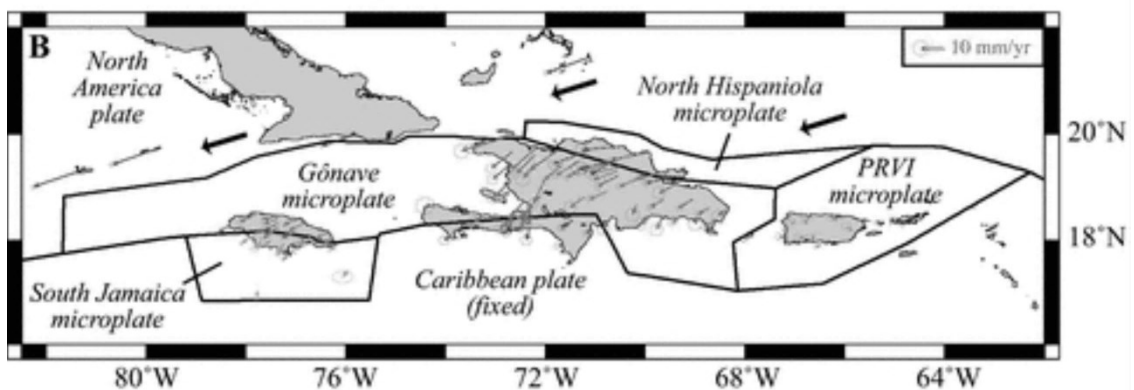


Figure 10. Caribbean microplates. (Benford, 2012).

From the geological point of view, the peninsula is constituted by two main lithological groups: Samaná metamorphic complex, a subduction-related formed by a dipping imbricate stack of high-P metasedimentary Mesozoic rocks; and sedimentary covers formed by silicates and carbonate material from Miocene, Miocene-Pleistocene and Holocene age (SGN, 2010).

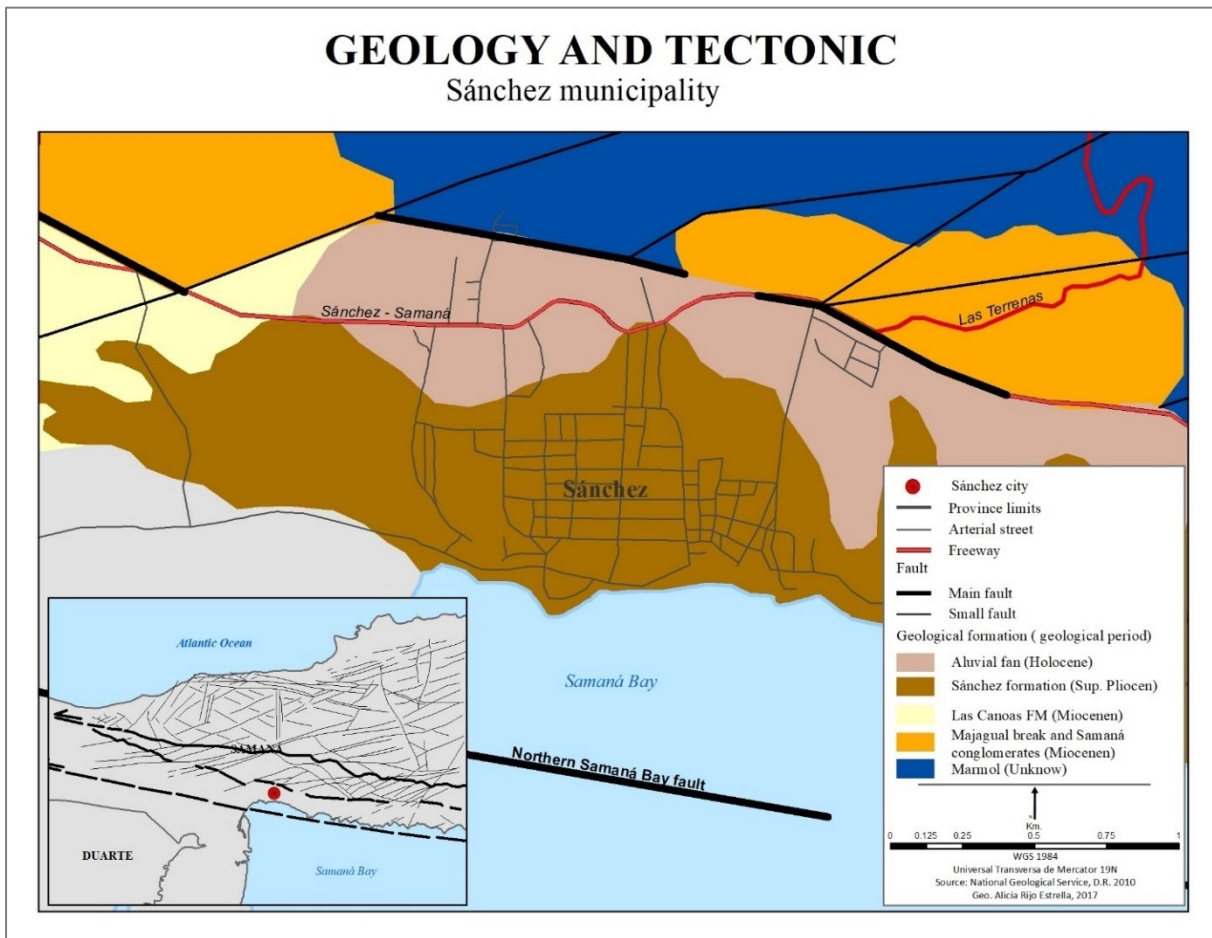


Figure 11. Geology and tectonic map.

The AOI is located in Sánchez Formation, defined by Douglas Robertson and Associates in 1981, during its exploration of coal in the zone required by Rosario Dominicana Mine. It is dominated by mudstone, lignite coal and organic-rich mudstones (Joyce, 1991). Its presumed age is Pliocene or younger.

Sánchez Formation is located in the meridional border of Samaná Sierra, the AOI, which lies completely on top of it, stratigraphically west of Sánchez is on top of Las Canoas Formation and

east on top of Samaná Conglomerates. Samaná Conglomerate, is composed of marble and other metamorphic clasts, is dominated by thick bedded of approximately 0.5 to 2.5 m conglomerates with intercalations of Sandstones (Joyce,1991, Llinas,1983), on the other hand, Las Canoas Formation is constituted by conglomerates composed of metamorphic clast and macrofossils.

The slope where the city rest is slightly wavy from 4-8%, it faces Samaná Sierra with slopes from 16 to 32%. Because of its geological and tectonic characteristic, the AOI is susceptible to instability causing problems in building, houses and roads. In the figures Figure 12 and Figure 13, a series of segments where construct in order to visualize, with the proper resolution limitations, the elevation profile of the AOI.

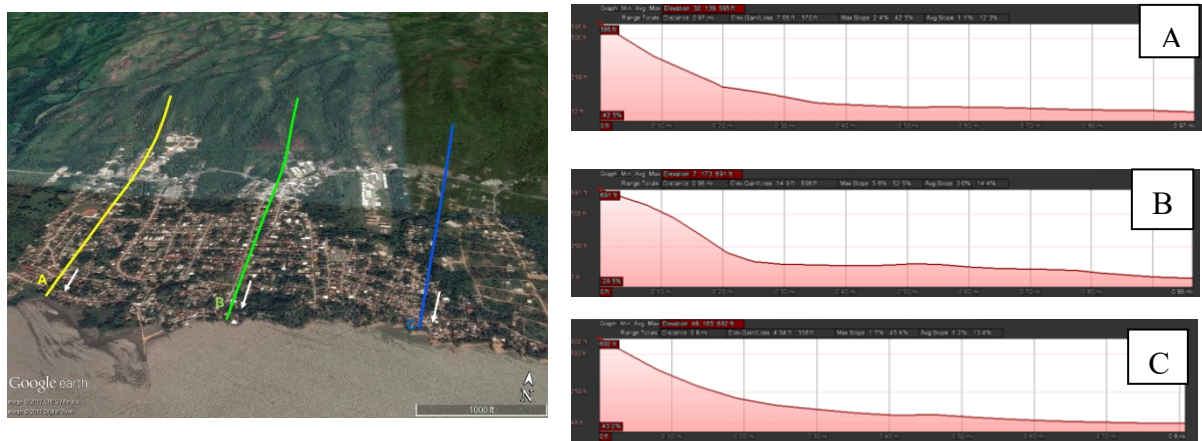


Figure 12. Vertical segment elevation profile, where white arrows indicate the direction of the segment.

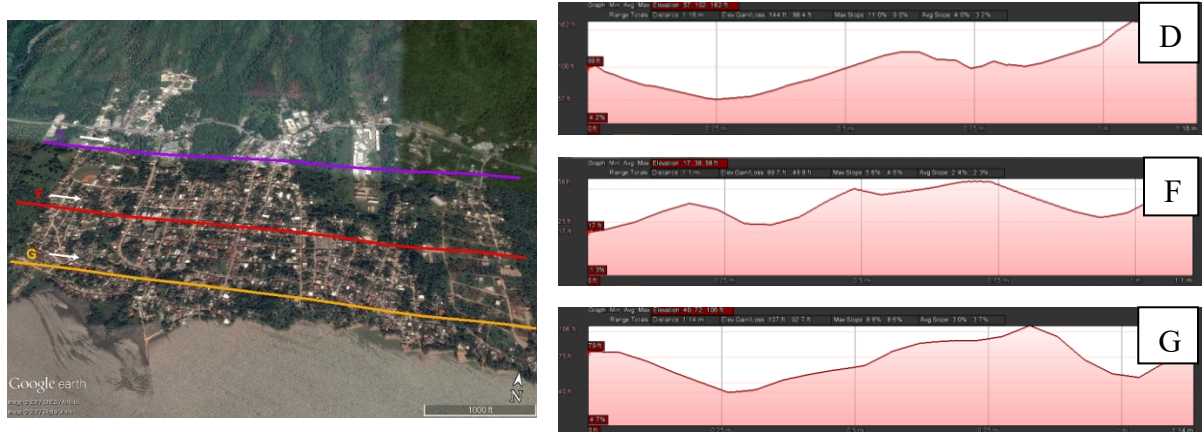


Figure 13. Horizontal segment elevation profile, white arrows indicate the direction of the segment.

In the vertical segments is easy to differentiates the mountainous areas with steep slopes from the deposition areas with gentle slopes. In case of horizontal segments, the curves of the slope are shown, displaying small hills and valleys.

6.1.2 Geomorphology settings

Historically Samaná peninsula used to be refed as a continuous island next to Hispaniola, as show in different maps Bowen (1747), Bellin (1758) and Tardieu (1802). According to these authors a marine canal used to exist in this area, that later was fill with sediments from Yuna river.

Its current appearance has been outlined mainly during the Pliocene and Quaternary, from definitive lifting of the peninsula and its tilting to the north, very possibly as a consequence of the most recent movement Northern Samaná Bay fault (SGN, 2010).

According to the Atlas of Biodiversity and Natural Resources publish by the Ministry of Environment and Natural Resources of Dominican Republic in 2012, the AOI is locate in marine lacustrine deposit delimited to the north by alluvial fans product of physical and chemical weathering of limestones and conglomerates from Samaná Sierra. south Samaná Bay and West Swap product of the Yuna river.

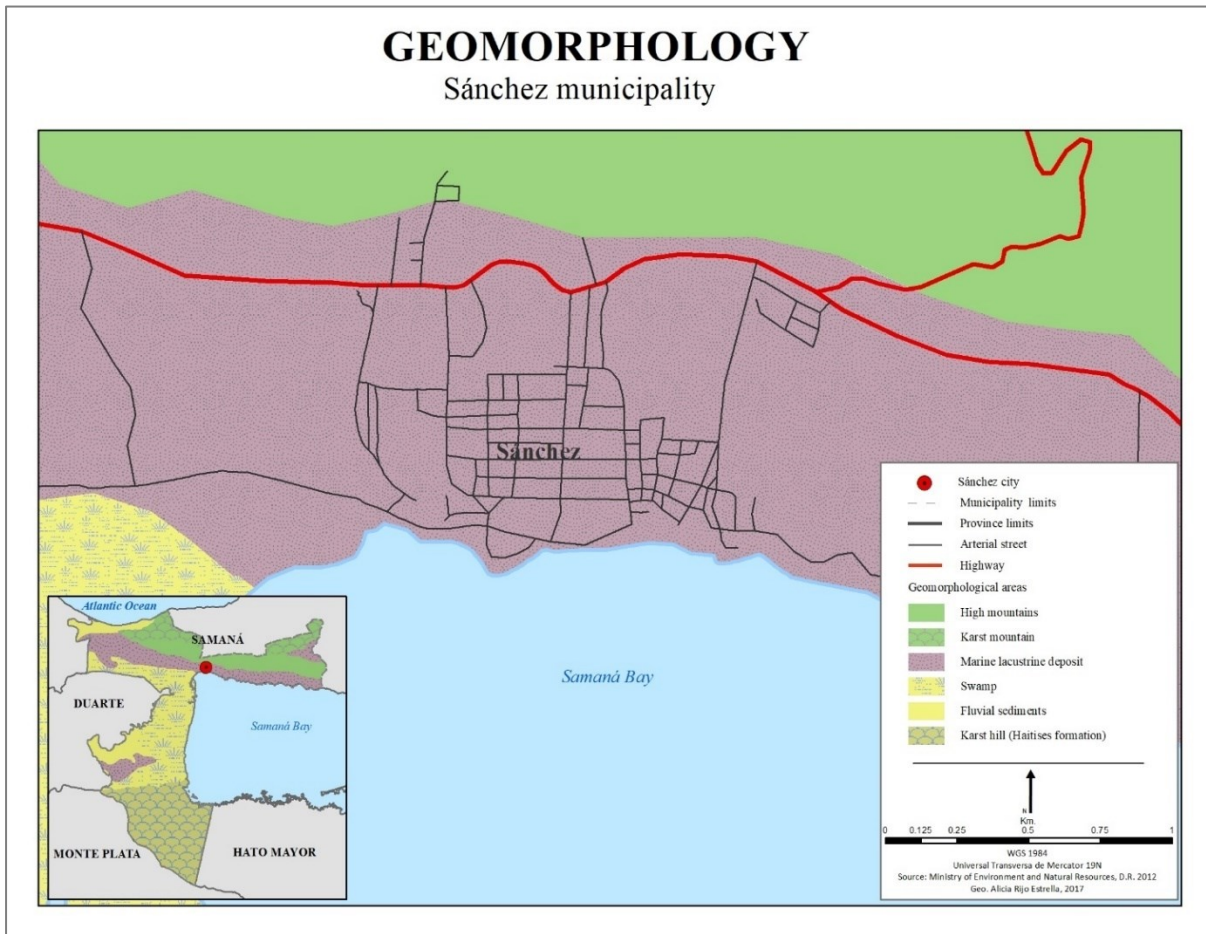


Figure 14. Geomorphology map.

6.1.3 Climatology and Hydrography

Precipitation is one of the triggers for landslides occurrence and a factor of decorrelation due to atmospheric contribution, for this reason is necessary to understand the rain patterns in the AOI. For the climate analysis, Climatograph of 30 years interval were used, the data for their realization was provided by the Meteorological Office of Dominican Republic from the Sánchez meteorological station.

The lowest precipitation trend is between January and April, with rainfall lower than 150 mm per month. In May the pattern changes due to convective rains caused by northeaster Trade winds,

rainfall during June-October is more regular with intervals of 150 mm to 200 mm. November and December present increase above 200 mm.

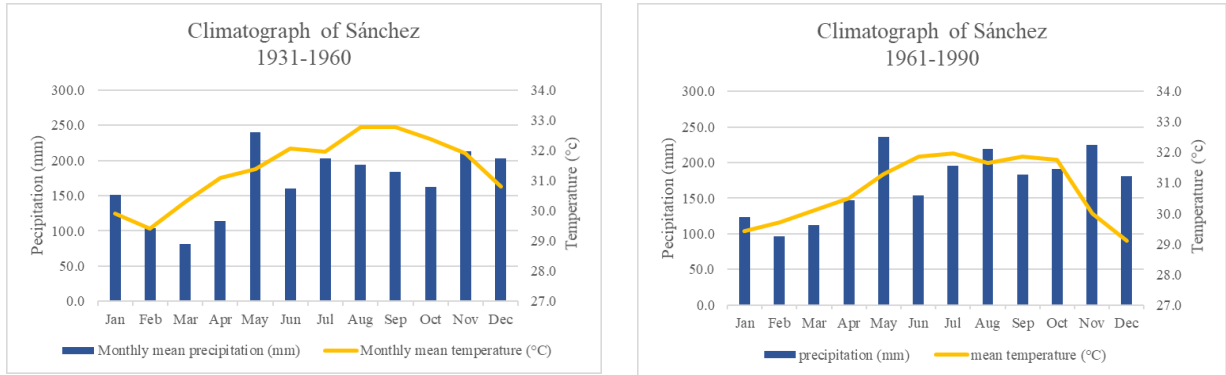


Figure 15. Climatograph Sánchez.

Due to its location in the tropical zone, change in temperature because seasons are not extreme, register temperature in the both Climatograph show a minimum of 29°C and maximum of 33°C approximately.

Table 6. List of tropical storms and hurricanes (2015-2017).

Year	Type		Name
	Tropical storm (winds speed 63 – 118 km/h)*	Hurricanes (winds speed 118 to >250 km/h)*	
2015	x		Erika
2016		x	Earl
2016		x	Hermine
2016		x	Matthew
2017		x	María
2017		x	Irma

*Saffir-Simpson scale.

Low pressure weather systems as hurricanes are common in the Caribbean, these phenomena contribute an incredible amount of rainfall and wind in a few hours, saturating the soils and destroying vegetation, agriculture areas and infrastructures. The hurricane season is between June 1st and November 30th. Some hurricanes and storms that has touched or pass nearby

Dominican Republic during the investigation period and cause some damage, can be seen in Table 6.

Superficial runoff waters in the peninsula are reigned by small to medium stream, born in Samaná Sierra, most of them seasonal and short. In the AOI, the stream El Gri-Gri is the only constant source of runoff waters.



Figure 16. El Gri-Gri, stream near landslide 2005.

6.2 Sánchez landslides

Once analyzed the geological, tectonic, geomorphological, climatological and hydrological setting of the AOI and review the landslides literature, is possible to determine that Sánchez is over a creep landslide.

A creep landslide is a very slow movement, occurring on gentle slopes because of the way soil particles repeatedly expand and contract in wet and dry periods. When wet, soil particles increase in size and weight, and expand at right angles. When the soil dries out, it contracts vertically. As a result, the soil slowly moves downslope (Rotaru et al, 2007).

Creep landslide phase is the activation of old landslides that took place due to tectonic activities. It is considered as a progressive action that provides signals of movement before it happens. In the AOI, the mudstones that constituted Sánchez formation slip on the hard formations of Las Canoas and Samaná Conglomerate. Moist trap in Sánchez F. leads to the chemical decomposition of the rock due to underground water that takes place in a previous develop plane of failure.

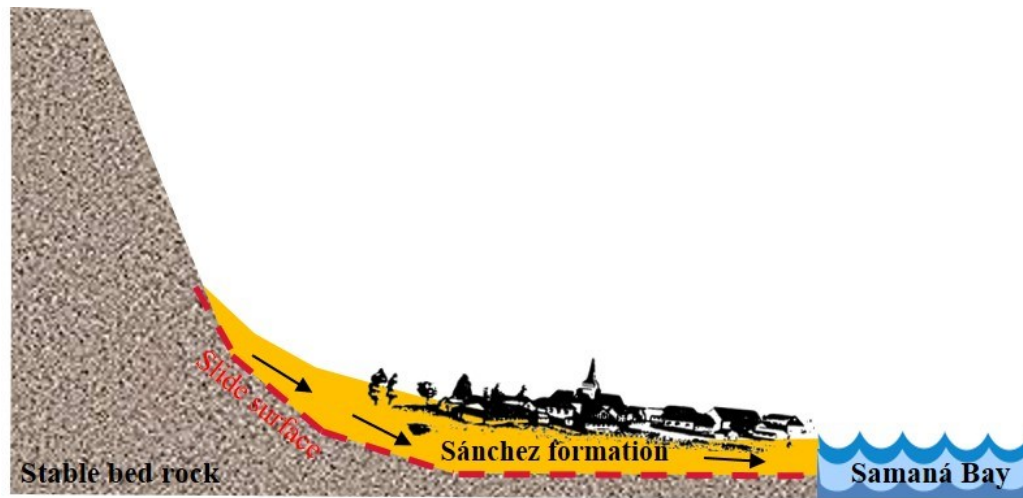


Figure 17. AOI creep landslide diagram.

When the state of decomposition reaches a level, the shear strength of the slip layer decrease, producing the move of the formation downhill, in the direction of the sea without the failure of the whole slope, however, in places where the pressure and stress continuous, failure is to be expect.

In the AOI, creep landslide is influence by seasonal rainfall, hurricanes and tropical storms, that constantly add moist to the underground, keeping the creep landslide active. Is also important to mention the anthropogenic effects of the urban development, like:

- Lack of planning about drinking and waste waters: clean water is carried by underground PVC pipes that, due to the movements, break and produce leakages, these splits are hard to detect producing a saturation of the soil. In the case of waste waters, these are

contained in a first stage in concrete boxes that retains hard materials but let waste water to infiltrate.

- Destruction of natural drainage: small streams were destroyed in order to adequate the terrain for new structures.
- Changes in the infrastructure: typical wood and tin houses where substitute by concrete houses and buildings up to 4 levels generating higher pressure due to weight. Apartment blocks were built by the government to refuges of 2005 movements.



Figure 18. Typical house in Sánchez.



Figure 19. Apartment blocks build for refugees.

- Change in vegetation: change of natural vegetation in mountainous areas to coconut palm tree, which has superficial roots and reduce cohesion of the soil.



Figure 20. View of the mountains near AOL.

6.2.1 Field observations

In 2005 an important landslide took place, destroying houses completely and damaging others; Infrastructures as roads were also damage, causing problems in communication between the peninsula and main land. Around 10 families lose their homes, forcing the government to relocate them.



Figure 21. Damage infrastructure during 2005 landslide.

After that disaster, small and continuous movements took place in the city, unfortunately without a proper registration of the events location. In December 2016, it was possible to perceive the damage caused by the last mass movement, approximately 10 houses were destroyed. According to owners and neighbors the event occurs during night, giving some warnings of movement that allowed the habitants to evacuate the houses in time and avoiding any human lost..





Figure 22. Affected area during 2016 landslide.

Sing of landslides can be visible in Google Earth™ scenes when comparing 2014 and 2017, (Figure 23)



Figure 23. Affected area in 2016, before and after landslide.

7 PSINSAR ANALYSIS

After review important concepts and limitations of PSInsar, and get background information of the AOI, is time to proceed with the analysis. The software used were SARPROZ © and ArcGIS.

7.1 Available SAR data

The available data for ground deformation analysis of the area consist in 41 Descending and 37 Ascending orbits SENTINEL-1 Wide Swath Mode Level 1 SLC scenes, from January 2015 to August 2017. For Descending mode, the time interval average was 24 days, while the Ascending mode was 21 days. The total storage needed in this investigation was 306.54 GB.

Table 7. List of scenes.

Descending						Ascending					
Code	Date	Interval (days)	Code	Date	Interval (days)	Code	Date	Interval (days)	Code	Date	Interval (days)
D1	09-01-15	0	D22	07-08-16	24	A1	22-07-15	0	A22	17-02-17	12
D2	26-02-15	48	D23	31-08-16	24	A2	08-09-15	48	A23	13-03-17	24
D3	22-03-15	24	D24	24-09-16	24	A3	02-10-15	24	A24	25-03-17	12
D4	15-04-15	24	D25	29-12-16	96	A4	19-11-15	48	A25	06-04-17	12
D5	09-05-15	24	D26	15-02-17	48	A5	13-12-15	24	A26	18-04-17	12
D6	02-06-15	24	D27	27-02-17	12	A6	06-01-16	24	A27	30-04-17	12
D7	26-06-15	24	D28	11-03-17	12	A7	30-01-16	24	A28	12-05-17	12
D8	20-07-15	24	D29	23-03-17	12	A8	23-02-16	24	A29	24-05-17	12
D9	13-08-15	24	D30	04-04-17	12	A9	18-03-16	24	A30	05-06-17	12
D10	06-09-15	24	D31	16-04-17	12	A10	11-04-16	24	A31	17-06-17	12
D11	30-09-15	24	D32	28-04-17	12	A11	05-05-16	24	A32	29-06-17	12
D12	24-10-15	24	D33	10-05-17	12	A12	27-06-16	53	A33	11-07-17	12
D13	17-11-15	24	D34	22-05-17	12	A13	09-08-16	43	A34	23-07-17	12
D14	04-01-16	48	D35	03-06-17	12	A14	02-09-16	24	A35	04-08-17	12
D15	28-01-16	24	D36	15-06-17	12	A15	26-09-16	24	A36	16-08-17	12
D16	21-02-16	24	D37	09-07-17	24	A16	20-10-16	24	A37	28-08-17	12
D17	16-03-16	24	D38	21-07-17	12	A17	13-11-16	24			
D18	09-04-16	24	D39	02-08-17	12	A18	07-12-16	24			
D19	03-05-16	24	D40	14-08-17	12	A19	31-12-16	24			
D20	27-05-16	24	D41	26-08-17	12	A20	24-01-17	24			
D21	14-07-16	48				A21	05-02-17	12			
Average Interval		24				Average Interval		21			

this reason is necessary to know the days with precipitation and avoid its usage as Master. Weather data was obtained through Wunderground API.

- **Area selection:** scenes covers a large area, processing all of it would have cause an unnecessary demanding process, therefor, the area of interest was selected using the coordinates near its center. Due to the amount of vegetation and sea in the AOI, the selection area was done with a buffer of 20 km², this way other consistent scatters could be used as well.
- **Master scene selection:** for the Coregistration to be as accurate as possible as well as measurements, a scene between the initial and end date scene was taken, this way the temporal decorrelation was reduce. It is also important the no precipitation, due to reasons previously mention.
- **Reflectivity map and Coregistration:** the reflectivity map is the result of the average of all scenes of the dataset reflective pixels. The averaging operation has strongly suppressed the noise, enhancing all targets which kept stable reflectivity throughout the dataset (Perissin, 2014). Reflectivity maps of the data set are present in Figure 25 and Figure 26. The Coregistration refers to the process of alignment of two SAR scenes, so that corresponding pixels in the two scenes contain the same portion of imaged terrain (Perissin, 2014). One scene is taken as reference grid while the rest are resembled around it, reference scene is called Master and rest Slaves. This step minimizes the effects of spatial and temporal baselines, maximize the total coherence of the interferometric stack and keep as low as possible the dispersion of the normal baseline values (Tofani, 2013).

InSAR process takes place after the previous SAR computation, using the coregistered scenes is possible to create the interferometry between scenes, the steeps took were:

- **Interferogram generation:** consist in reassemble of 2 scenes, the Master and a Slave with a low B_n . Flattering and DEM removal were used to help estimate the contribution of geometry.
- **Filtering:** the filtering algorithm used was Goldstein in a 10 x 10 window. The phase unwrap process was neglected because displacement can be observed without it.

- **PS generation:** PS were generated using a thresholding of amplitude stability index $1-\sigma/\mu > 0.7$ in the reflectivity map, scatters with high coherence where mostly concentrated in the urban area where reflectivity is elevated and consistent, this was expected since nearby mountains and sea coherence is by default really low. Using a reference point, it was possible to estimate the linear trend and height in a range of -50 to 50. The multi-interferometric analysis generates displacement time-series for individual radar target, generally assuming a linear model of deformation.
- **Atmospheric phase removal:** Because of the incidence of tropical storms, hurricanes and normal rainy season in the AOI during most of the year, was important to estimate the atmospheric contribution. In this case, information from the meteorological station in Sánchez was used.
- **Geocoding:** the geocoding step is basically too export the result data to csv format. This data will be then use in ArcGIS to produce deformation velocities and displacement rate maps.

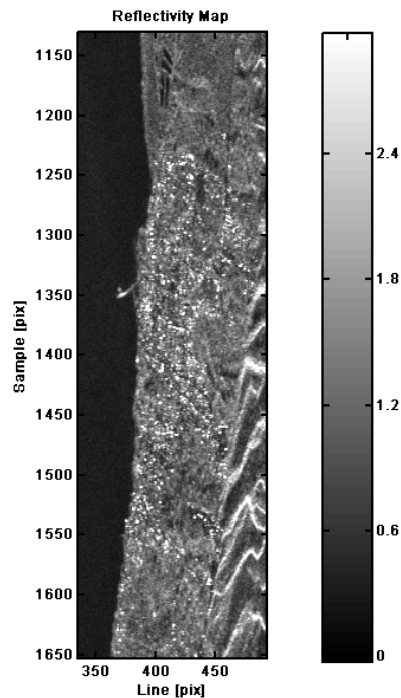


Figure 25. Reflectivity map Ascending orbit.

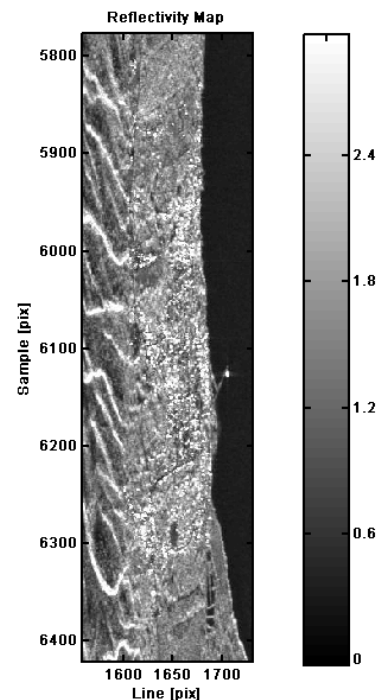


Figure 26. Reflectivity map Descending orbit.

ArcGIS process:

Generation of displacement and velocity maps were processed in ArcGIS software, the general steps are described below:

- **Cleaning of dataset:** The PS located outside of the AOI were removed from the data set, the main reason is that mostly this PS has a low coherence due to the vegetation around the AOI, so its usage can only lead to miss calculations.
- **Elaboration of deformation velocity in LOS maps:** is constituted by the PS velocity results in the LOS. The results were classified in speeds: <-3 ; -2.9 to -3 ; and >3 .
- **Elaboration of cumulative displacement maps:** Inverse Distance Weighted (IDW) interpolation method was used to create the maps of InSAR cumulative displacement for the AOI using the PS displacement data. IDW weights the average values available to estimate the values in unknown places, based in the first principle of geography: close objects have similar attributes.

7.3 PSInSAR results

The AOI can be considered a complex processing site, where geological, geomorphological and tectonic backgrounds are briefly studied and explained. This area also has the characteristics of have a small extension of 2 km² surround by steep mountains and ocean, both scenarios impossible to applied InSAR methods due to geometrical distortions and temporal and spatial decorrelation. Inside of the urban areas there are also influence of parks, alleys and presence of trees that induce volume scattering, therefore the PS points density is low.

Deformation velocities of each PS is calculated based on the LOS of the satellite in Ascending (S-N) and Descending (N-S) orbits. The combination of both orbits makes possible the observation of the same point on the earth's surface from two different perspectives, hence calculate vertical and horizontal motion. The direction of the slope in Sánchez is NE-SW.

To understand the results is necessary to know what the values mean in InSAR, when a vertical ground displacement take place, both ascending and descending orbit present negative values, moving away from the sensor. In case of horizontal motion, the vector will be exchange, with one positive and other negative. Positive velocities indicate surface deformation motion upward and eastward, while negative deformation rates reflect movements downward and westward (Tofani et al, 2013). The deformation velocity of the PS in the ascending and descending orbits where classified in: $<-3\text{mm/year}$, between -3mm and 3 mm per year and $>3\text{mm/year}$.

In Figure 27, is possible to appreciate that Ascending orbits has most of the terrain is in the “stable or not significant” movement range, between -3mm and 3 mm per year , with insolate areas with more or less horizontal movements (values $>3\text{mm/year}$), is interesting to notice a specific area that present several PS with values $<-3\text{mm/year}$ located near the sea. The East part of the AOI is in urbanization development process, therefore the amount of vegetation is significantly, this could explain the lack of PS in the area.

For descending orbit (Figure 28), the results are very interesting, the patter registered is pretty alike to the slopes observed in 6.1.1, even though topography has been estimated and remove

from the interferogram. In depression areas values present negative values, while higher areas have stable values, zones with previous deformation (mark in red rectangle) have positive.

When comparing both results for Ascending and Descending data, the first impression is a complete decorrelation between them, however, there is certain correlation, locations mark with red rectangles are those with history of motion occurrence. Rectangle #1, represent the location of the failure occurred in 2005 in “El Play” neighborhood and rectangle #2, is the second failure in 2016, in “Pueblo Arriba” neighborhood. For area #1, the Ascending and Descending orbits shows slope stability, this can be explained because the slip layer reach its breaking point in 2005, now is in rest and accumulation pressure once again. For the area #2, the scenario is different, this location experienced deformation during the course of this investigation so detection of movement is expected. In ascending orbit, the area shows stable values (between -2.99 and 3 mm/year), while in Descending orbit present move towards the satellite. This difference between both orbits can represent a horizontal movement. A third interest area #3 can be appreciated in “Los Rieles” where both orbits detect vertical movement.

Cumulative displacement values are highly correlate with the velocity of the scatter; hence one cannot happen without the other, is also for some people easier to interpreted. Focusing in the previous mention areas where motion was detected, the cumulative displacement #1, present positive values in both orbits. In case of the neighborhood “Pueblo Arriba”, the displacement in Ascending orbit is between 0 and 5 mm/year with a small peak, for Descending the values are from 10 to 20 mm/year. The area #3, present negative displacements in both orbits.

Table 8. PSInSAR summary results.

Orbit	Ascending	Descending
Temporal range	22-07-15 to 28-08-17	09-01-15 to 26-08-17
No. of Scenes	37	41
No. PS	269	290
Mean velocity (mm/year)	1.24	1.27
Min. velocity (mm/year)	-4.6	-14.5
Max. velocity (mm/year)	5.9	9.9
Mean Cumulative displacement (mm/year)	2.5	3.30

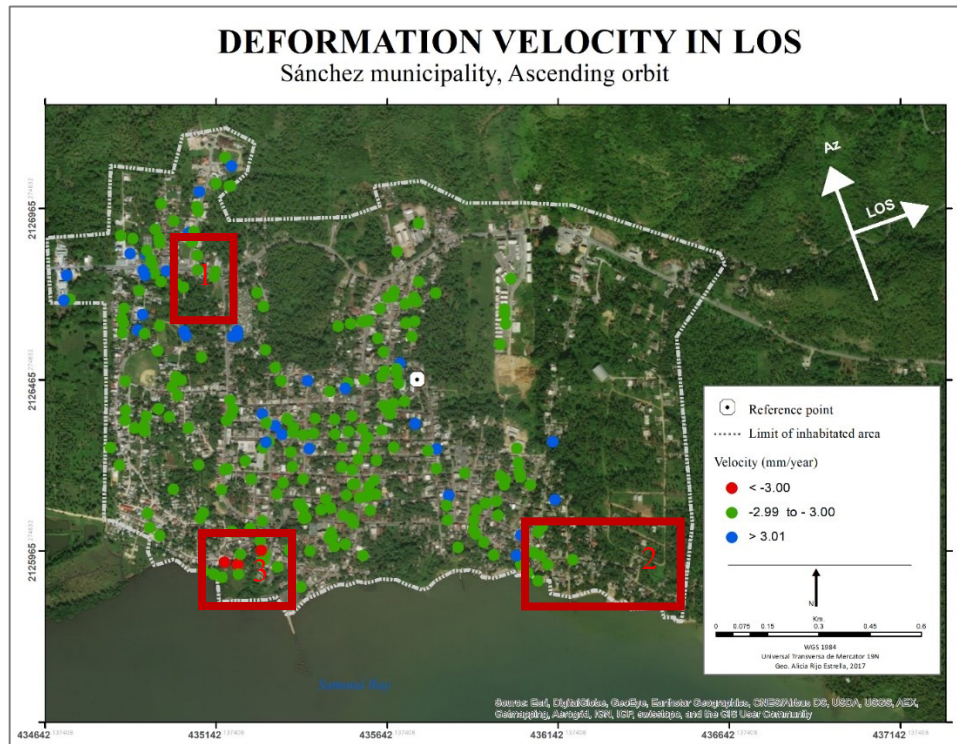


Figure 27. Deformation velocity in Line of Sight (LOS). Ascending orbit.

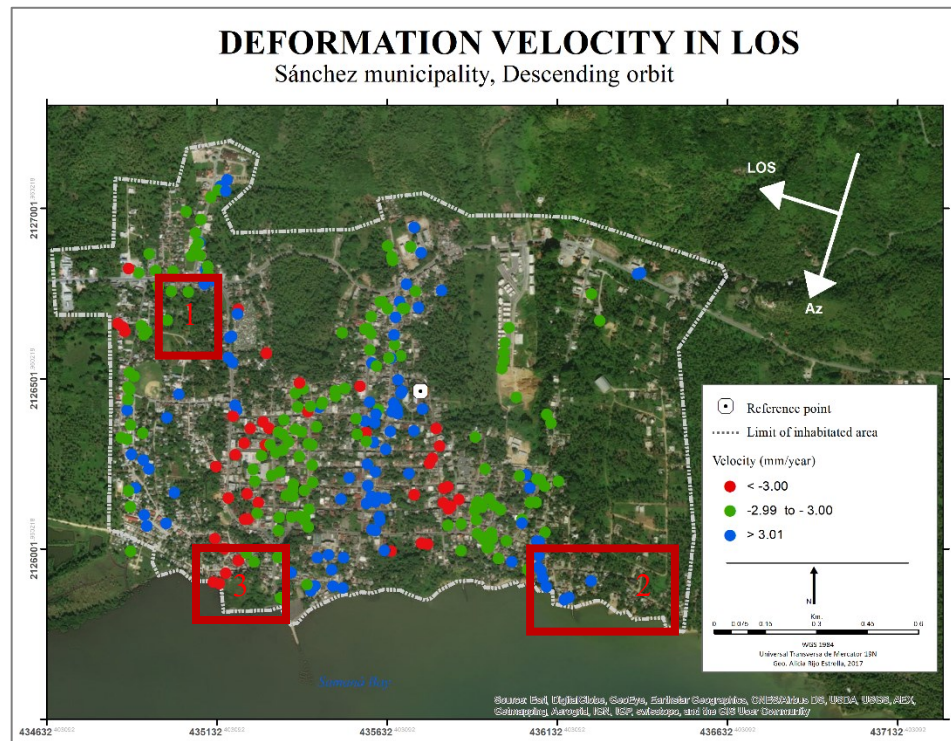


Figure 28. Deformation velocity in Line of Sight (LOS). Descending orbit.

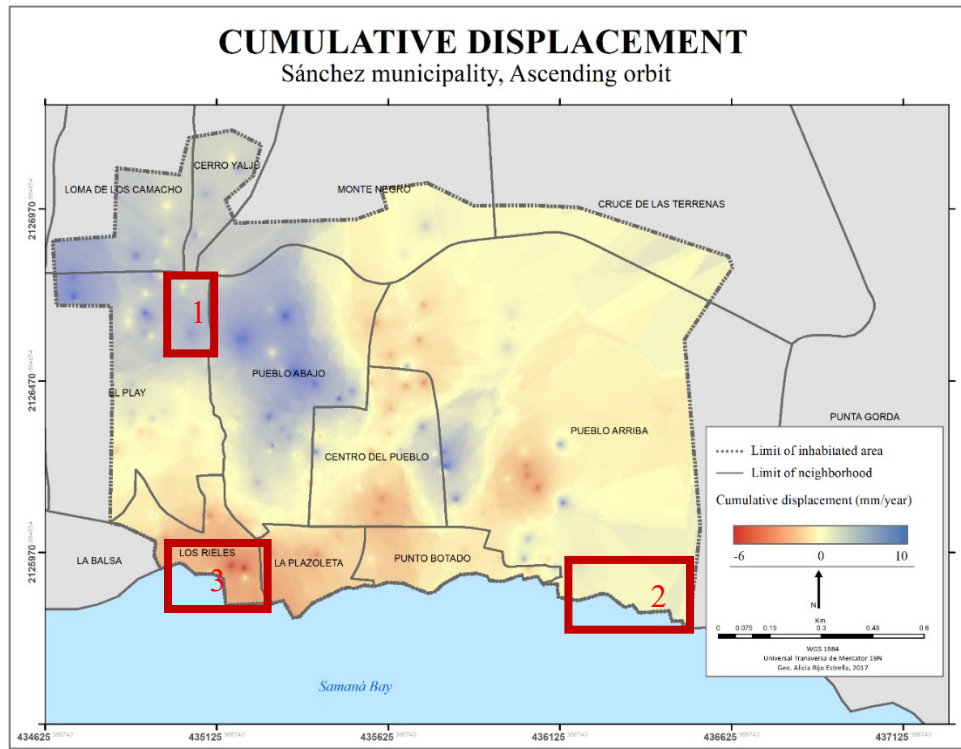


Figure 29. Cumulative displacement, Ascending orbit.

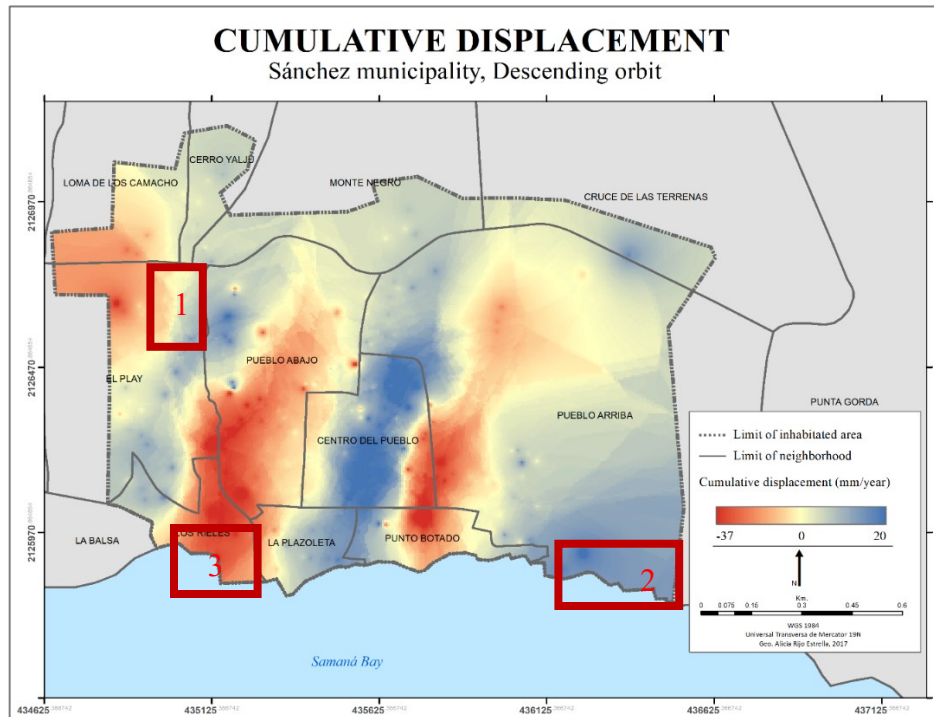


Figure 30. Cumulative displacement, Descending orbit.

8 CONCLUSION AND RECOMMENDATIONS

8.1 Conclusion

The utilization of InSAR for landslide identification is a promising technology able to measure motion displacement in millimeter scale, the main advantage of it is the possibility to process large areas, that with common ground detection methods will be hard or even impossible. Usage of continuous bright stable elements on the earth's surface, also known as Persistent Scatters, makes possible the measurement in urban and rocky areas.

However, is important to consider that this wonder has to overcome limitations that can affect the outcome or even make the data impossible to process. The main restrictions of InSAR is called decorrelation and is induced by several factors develop in the body of the thesis. Specifically, for landslides monitoring there are also extra consideration as: deformation velocity rate can't be too big because it can be considered as error, data acquisition period must be small and the Line Of Sight (LOS) of the sensor have to be perpendicular to the motion in order to be capture.

PSInSAR technique was performed using SENTINEL-1 data over Sánchez municipality in a period of 31 months. The Area Of Interest (AOI) was recognized as a creep landslide, the availability of the data was in periods of 21 to 24 days for both Ascending and Descending orbits, making the analysis feasible.

After the application of Interferometry in Sánchez municipality, it was possible to identify deformation velocity in the LOS and cumulative displacement and make the pertinent cartography. Known areas with historic motion as well as field observations were used to validate the results.

The thesis objectives were achieved by:

Achieve theoretical background of InSAR techniques, with the main focus on Persistent Scatters (PS) and specifics of InSAR towards investigating landslide activity: I have collect and

interpreted knowledge from different publications, books, official reports and dissertations about the topic of the research.

Perform PS processing of SENTINEL-1 data over Sánchez municipality: processing took place using SARPROZ software.

Evaluate achieved results: outputs were interpreted and analyzed, finding similarities between detected movements with ground truth information.

Created map of potential slow landslide activity: cartography of outputs was present, where is possible to observed deformation velocity rate and cumulative displacement.

8.2 Recommendations for future work

For future investigation, I considered that is necessary to take actions:

- Utilization of corner reflector that works as a reflective guide in urban areas surround by vegetated areas, the reflector must be set outside of the landslide area, which must be identify by an expert geologist.
- Usage of GNSS traditional ground methods for comparison, like: GPS measurements and accelerometer.
- Usage, if possible of another wavelength band as L band. For this case the result may be a little better because the L band is not affected by volume scatters.

3 BIBLIOGRAPHY

Books

- Comer, D. C. & Harrower, M. J. Mapping archaeological landscapes from space. (Springer, 2013).
- Daniele Perissin. Interferometric SAR Multitemporal Processing: Techniques and Applications. Chapter 8 from Yifang Ban. Multitemporal remote sensing, methods and applications. (Springer, 2017).
- Hein, A. Processing of SAR data: fundamentals, signal processing, interferometry. (Springer-Verlag, 2010).
- James Joyce. Blueschist metamorphism and deformation on the Samaná Peninsula; A record of subduction and collision in the Greater Antilles. From Mann, P., Draper, G. & Lewis, J. F. Geologic and tectonic development of the North America-Caribbean plate boundary in Hispaniola. (Geological Society of America, 1991).
- Ketelaar, Virginia Bernard H. Satellite radar interferometry: subsidence monitoring techniques. (Springer, c2009).
- M. Simons and P. A. Rosen. Interferometric Synthetic Aperture Radar Geodesy. (Elsevier B.V., 2007).
- Ramon F. Hanssen. RADAR Interferometry, Data Interpretation and Error Analysis. (Kluwer academics publishers, 2001).
- Richards, J. A. Remote Sensing with Imaging Radar. (Springer Berlin, 2009).
- Thomas M. Lillesand, Ralph W. Kiefer, Jonathan W. Chipman. Remote Sensing and Image Interpretation. (Wiley, 2008).
- Wasowski, K., Bovega, F. Investigating landslides and unstable slopes with satellite Multi Temporal Interferometry: Current issues and future perspectives. (Engineering Geology, 2014).

Scientific papers

- Ancuța Rotaru, Daniel Oajdea and Paulică Răileanu. “Analysis of the Landslide Movements”. International Journal of Geology, volume 1, (2007).
- Benford, B., Demets, C. & Calais, E. “GPS estimates of microplate motions, northern Caribbean: evidence for a Hispaniola microplate and implications for earthquake hazard”. Geophysical Journal International 191, 481–490 (2012).
- Crosetto, O. Monserrat, A. Jungner, B. Crippa. “Persistent Scatterer Interferometry: Potential and Limits”. Satellite Radar Interferometry Remote Sensing and Digital Image Processing 27–49 (2009).
- Ding, X.-L., Li, Z.-W., Zhu, J.-J., Feng, G.-C. & Long, J.-P. “Atmospheric Effects on InSAR Measurements and Their Mitigation”. Sensors 8, 5426–5448 (2008).
- L. Choo, Y. K. Chan, and V. C. Koo. “Geometric Correction on SAR Imagery”. (2012).
- Tengting Qu, Ping Lu, Chun Liu *, Hangbin Wu, Xiaohang Shao, Hong Wan, Nan Li and Rongxing Li. “Hybrid-SAR Technique: Joint Analysis Using Phase-Based and Amplitude-Based Methods for the Xishancun Giant Landslide Monitoring”. Remote Sensing 8, 874(2016).
- Veronica Tofani *, Federico Raspini, Filippo Catani and Nicola Casagli. “Persistent Scatter Interferometry (PSI) Technique for Landslide Characterization and Monitoring”. Landslide Science for a Safer Geoenvironment 351–357 (2014).
- Varnes, D.J. and Cruden D.M., “Landslide Types and Processes, Special Report, Transportation Research Board”. National Academy of Sciences, 247:36-75 (1996).
- Zhang, Y. “A comparison of the different models used for interferograms flattening”. Proceedings. 2005 IEEE International Geoscience and Remote Sensing Symposium, 2005.

Dissertation

- Bähr, H. Orbital Effects in Spaceborne Synthetic Aperture Radar Interferometry. (2013).
- Milan Lazecký. Monitoring of Terrain Relief Changes using Synthetic Aperture Radar Interferometry. (2011).

Reports

- European Space Agency. SENTINEL-1 User Handbook (2013). Retrieved August 2017, from https://sentinel.esa.int/documents/247904/685163/Sentinel-1_User_Handbook.
- European Space Agency. InSAR Principles: Guidelines for SAR Interferometry Processing and Interpretation (2007). Alessandro Ferretti, Andrea Monti-Guarnieri, Claudio Prati, Fabio Rocca. Retrived May 2017, from <https://pdfs.semanticscholar.org/6b85/85741947513c954c941de1f11033070ae7f3.pdf>
- Food and Agriculture Organization of the United Nations (FAO). FAO watershed management field manual, landslide prevention measures (1988).
- Highland, L.M., Bobrowsky, Peter. The Landslide Handbook- A guide to understanding landslides. (United States Geological Survey and Geological Survey of Canada, 2008). Retrieved August 2016, from https://pubs.usgs.gov/circ/1325/pdf/C1325_508.pdf
- Oficina Nacional de Estadística de la República Dominicana. IX Censo Nacional de población y vivienda (2010). Retrieved August 2017, from <https://www.one.gob.do/Categoria/Redatam/>
- Servicio Geológico Nacional de la República Dominicana. Memoria Mapa geológico de la Republica Dominicana, hoja Sánchez (6273-1), (2010).

4 NOMENCLATURE

List of symbols

Operator	Meaning
λ	wavelength
r	range
B_n	baseline
θ	incidence angle
E	Expect value
ϕ	phase
$\Delta\phi$	Phase difference
$\Delta\phi_{geom}$	Geometry phase contributor
ϕ_{defo}	Deformation phase contributor
ϕ_{atmo}	Atmospheric phase contributor
ϕ_{noise}	Noise phase contributor
z_1	complex interferogram
D	displacement vector
γ	coherence
γ_N	Radar system and processing decorrelation
γ_G	Geometry decorrelation
γ_Z	Volume decorrelation
γ_T	Time decorrelation
Δh_a	altitude ambiguity
$\delta\phi_{topo}$	Topography error
$\delta\phi_{orb}$	Orbit error

List of abbreviations

Abbreviation	Meaning	Abbreviation	Meaning
AOI	Area of interest	SLC	Single look complex
DEM	Digital Elevation Model	SM	Stripmap
DInSAR	Differential InSAR	TEC	Electron content
EW	Extra Wide swath	TOPSAR	Terrain Observation with Progressive Scanning SAR
GIS	Geographic Information System	WV	Wave
GRD	Ground Range Detected		
IW	Interferometric Wide Swath		
LOS	Line of Sight		
PS	Persistent Scattered Pixel		
RADAR	Radio Detection and Ranging		
SAR	Synthetic Aperture Radar		
SRTM	Shuttle Radar Topography Mission		

5 LIST OF FIGURES

Figure 1. SAR geometry.....	4
Figure 2. SAR synthetic antennas schema.....	4
Figure 3. SENTINEL satellite	6
Figure 4. Polarization with respect of the incident angle and surface (Richards, 2009).	9
Figure 5. Common scattering mechanisms (based in Richards,2009).	11
Figure 6. Topographic distortions.	12
Figure 7. InSAR geometry.....	13
Figure 8. Measurement of motion.	29
Figure 9. Localization map.....	30
Figure 10. Caribbean microplates. (Benford, 2012).....	31
Figure 11. Geology and tectonic map.....	32
Figure 12. Vertical segment elevation profile, where white arrows indicate the direction of the segment.....	33
Figure 13. Horizontal segment elevation profile, white arrows indicate the direction of the segment.	33
Figure 14. Geomorphology map.....	35
Figure 15. Climatograph Sánchez.	36
Figure 16. El Gri-Gri, stream near landslide 2005.	37
Figure 17. AOI creep landslide diagram.	38
Figure 18. Typical house in Sánchez.....	39
Figure 19. Apartment blocks build for refugees.....	39
Figure 20. View of the mountains near AOI.	39
Figure 21. Damage infrastructure during 2005 landslide.	40
Figure 22. Affected area during 2016 landslide.	41
Figure 23. Affected area in 2016, before and after landslide.	41
Figure 24. Workflow.	43

Figure 25. Reflectivity map Ascending orbit.	45
Figure 26. Reflectivity map Descending orbit.....	45
Figure 27. Deformation velocity in Line of Sight (LOS). Ascending orbit.	49
Figure 28. Deformation velocity in Line of Sight (LOS). Descending orbit.....	49

6 LIST OF TABLES

Table 1. Common SAR frequency bands and uses.	8
Table 2. Backscattering parameters.....	11
Table 3. Phase delay according to atmospheric conditions.	17
Table 4. Slope movements respect to the slide velocity.....	27
Table 5. Classification of slope movements.	27
Table 6. List of tropical storms and hurricanes (2015-2017).	36
Table 7. List of scenes.	42
Table 8. PSInSAR summary results.	48